**THE EUROPEAN
PHYSICAL JOURNAL C**

Greybody factors for massive scalar field emitted from black holes in dRGT massive gravity

Petarpa Boonserm[1,a], **Sattha Phalungsongsathit**[2,b], **Kunlapat Sansuk**[1,c], **Pitayuth Wongjun**[3,d]

[1] Department of Mathematics and Computer Science, Faculty of Science, Chulalongkorn University, Bangkok 10330, Thailand
[2] Physics Program, Faculty of Science, Chandrakasem Rajabhat University, Bangkok 10900, Thailand
[3] The Institute for Fundamental Study "The Tah Poe Academia Institute", 2nd Floor, Mahathamracha Building A, Naresuan University, Mueang Phitsanulok 65000, Thailand

Abstract Greybody factors are transmission probabilities of the Hawking radiation, which are emitted from black holes and can be obtained from the gravitational potential of black holes. The de Rham, Gabadadze, and Tolly (dRGT) massive gravity is one of the gravity theories that modified general relativity. In this paper, we investigate the greybody factor from the massive scalar field in both the asymptotically dS and the AdS spacetime using the WKB and the rigorous bound methods. We found that the greybody factor depends on the shape of the potential as found in quantum mechanics. The higher the potential barrier, the lower the amount of the greybody factor. Interestingly, for the low multipole case, we found that there exists a critical mass which provides the maximum bound of the greybody factor. This is a crucial feature of the massive scalar field on the greybody factor from the black holes in both the asymptotically dS and the AdS spacetime.

1 Introduction

A classical black hole can only absorb particles but not emit them. However, due to quantum effects, a black hole can create and emit particles from its event horizon, which can be seen as a thermal radiation called the Hawking radiation [1]. This radiation encounters the gravitational potential generated by the black hole itself. This results in the reflection and transmission of the Hawking radiation. Therefore, the actual spectrum observed by an asymptotic observer is different from a blackbody spectrum. A black hole greybody

factor is a quantity that describes the deviation of the Hawking radiation from a pure blackbody radiation.

There are various methods to compute the greybody factor. One of them is the general rigorous bound for reflection and transmission coefficients for one-dimensional potential scattering [2–4]. This formulation can be applied to a black hole greybody factor [5–21].

Almost all studies on greybody factor are conducted for massless scalar fields. The massive scalar field is expected to have a different behavior from the massless one in several astrophysical phenomena. For example, it was shown that the massive scalar field has less damping rate than the massless one in a Schwarzschild black hole background [22]. The mass of the scalar field can cause the instability of the scalar field itself [23,24] and the superradiant instability [25]. Unlike the massless scalar field, the quasi-normal modes from the massive scalar field can disappear, leaving undamping modes, which are called the quasi-resonance modes when the mass of the scalar field is more than some critical values [26].

Furthermore, the massive scalar fields play an important role in elementary particle physics. For example, in the Kaluza–Klein models, the behavior of a massless scalar field in the Fourier modes is similar to the massive one. In black hole spacetimes, the dynamic of the massive scalar fields become important [27]. In this work, we investigate the effects of the massive scalar fields on greybody factors.

One of the alternative theories of gravity is the massive gravity of which the main feature is to give mass to a graviton [28–33]. The ghost-free massive gravity in the four-dimensional spacetime and higher was achieved by de Rham, Gabadadze, and Tolley (dRGT) [34,35]. The black hole solutions and their thermodynamics in dRGT massive gravity were found in [36]. Moreover, the greybody factors

[a] e-mail: Petarpa.Boonserm@gmail.com

[b] e-mail: sattha.phalungsongsathit@gmail.com (corresponding author)

[c] e-mail: kunlapat11032540@gmail.com

[d] e-mail: pitbaa@gmail.com

for black holes in the asymptotically de Sitter (dS) spacetime in dRGT massive gravity were studied in [37].

In this paper, we generalize [37] to study the greybody factors for the massive scalar fields emitted from black holes in dRGT massive gravity. The dRGT massive gravity is outlined in Sect. 2. For the dRGT black hole, it is possible to have two horizons for the asymptotically dS spacetime and up to three horizons for the asymptotically AdS spactime. We parameterize the existence of the horizon by two model parameters $0 < \beta_m < 1$, $c_2 < 0$ for the asymptotically dS black hole and $1 < \beta_m < \sqrt{4/3}$, $c_2 > 0$ for the asymptotically AdS spacetime. The potentials of the dRGT black holes are derived in Sect. 3. We found that in addition to such two parameters, the potential depends on the scalar field mass. The behaviour of the potential is characterized by using these three parameters in this section. The greybody factors of the dRGT black holes are evaluated for both the rigorous bound and the WKB methods in Sect. 4. We found that the WKB method will be efficient for high potential or high multipole, while the results from the rigorous bound will still be valid for all range of parameters. However, the results from the rigorous bound can be approximated to ones from WKB only for the low frequency case. By analyzing the behaviour of the greybody factor, we found that it depends on the shape of the potential as found in quantum mechanics, specifically, the higher the potential barrier, the lesser the amount of the grebody factor. Moreover, for the low multipole case, we found that there exists a critical mass which provides the maximum bound of the greybody factor. Finally, the conclusions and discussions are given in Sect. 5.

2 dRGT black hole

One of the interesting ways to modify the theory of gravitation is by adding the graviton mass terms to general relativity which is usually known as massive gravity theory. There are several ways to provide the mass terms. However, most of them are not a good candidate since they encounter the ghost instabilities. Recently, the ghost-free massive gravity theory was proposed by de Rham, Gabadaze and Tolley called the de Rham–Gabadaz–Tolley (dRGT) massive gravity theory, which is represented by the action

$$S = \int d^4x \sqrt{-g} \left[\frac{M_P^2}{2} R[g] + m_g^2 (\mathscr{L}_2[g, f] + \alpha_3 \mathscr{L}_3[g, f] + \alpha_4 \mathscr{L}_4[g, f]) \right], \tag{1}$$

where α_3 and α_4 are model parameters. Note that R is a Ricci scalar, and m_g is a graviton mass. The interaction terms denoted by $\mathscr{L}_i$s are constructed with the fiducial metric $f_{\mu\nu}$

as

$$\mathscr{L}_2[g, f] = \frac{1}{2} \left([\mathscr{K}]^2 - [\mathscr{K}^2] \right) \tag{2}$$

$$\mathscr{L}_3[g, f] = \frac{1}{3!} \left([\mathscr{K}]^3 - 3[\mathscr{K}][\mathscr{K}^2] + 2[\mathscr{K}^3] \right) \tag{3}$$

$$\mathscr{L}_4[g, f] = \frac{1}{4!} \left([\mathscr{K}]^4 - 6[\mathscr{K}]^2[\mathscr{K}^2] + 3[\mathscr{K}^2][\mathscr{K}]^2 \right.$$
$$\left. + 8[\mathscr{K}][\mathscr{K}^3] - 6[\mathscr{K}^4] \right), \tag{4}$$

where the square bracket stands for the trace of a matrix such as $[\mathscr{K}] = g^{\mu\nu} \mathscr{K}_{\mu\nu}$. The tensor $\mathscr{K}_{\mu\nu}$ can be expressed as

$$\mathscr{K}_\nu^\mu = \delta_\nu^\mu - \mathscr{X}_\nu^\mu, \tag{5}$$

where $\mathscr{X}_\nu^\mu$ is defined by

$$\mathscr{X}_\alpha^\mu \mathscr{X}_\nu^\alpha = g^{\mu\alpha} f_{\nu\alpha}. \tag{6}$$

The form of the fiducial metric does not alter the existence of the ghost by construction. It is convenient to choose the form of the fiducial metric as [38–40]

$$f_{\mu\nu} = \text{diag}(0, 0, c^2, c^2 \sin^2 \theta), \tag{7}$$

where c is a constant. The static and the spherically symmetric black hole solution in the dRGT massive gravity is given by [37]

$$ds^2 = -f(\tilde{r})dt^2 + \frac{dr^2}{f(\tilde{r})} + r^2 d\Omega^2, \tag{8}$$

where $d\Omega^2 = d\theta^2 + \sin^2 \theta d\phi^2$, $\tilde{r} = r/c$,

$$f(\tilde{r}) = 1 - \frac{2\tilde{M}}{\tilde{r}} + \alpha_g(c_2 \tilde{r}^2 - c_1 \tilde{r} + c_0), \tag{9}$$

$\tilde{M} = M/c$, M is the black hole mass, $\alpha_g = m_g^2 c^2$ and c_0, c_1 and c_2 are dimensionless model parameters related to the parameters m_g^2, α_3 and α_4. By fixing α_g to be a positive constant, the c_2 characterizes the strength of the cosmological constant where it is negative/positive corresponding to the Schwarzschild de Sitter (SdS)/Schwarzschild Anti de Sitter (SAdS) solutions. The parameters c_0 and c_1 characterize the structure of the interaction terms, which determine the deviation from SdS (SAdS) solutions. Note that the dRGT solution reduces to SdS/SAdS solution in the limit $c_0 = c_1 = 0$. Since the parameter c is full, in this solution, it represents a length scale at which the theory manifests the effect of the gravitational modification for $r \gg c$, while the theory reduces to general relativity for $r \ll c$. Indeed, the parameter c is the Vainshtein radius in terms of the screening mechanism. In this paper, we focus on the case where the black hole has two horizons for the dRGT solution with asymptotically dS spacetime, and three horizons for the dRGT solution with asymptotically AdS spacetime. In order to characterize the existence of the horizons, it is convenient for us to choose

the parameter c_1 as [37]

$$c_1 = 3\sqrt[3]{4c_2^2}. \qquad (10)$$

Since the parameters are evaluated differently for the dRGT solution with asymptotically dS and AdS spacetime, we will separate our consideration into two subsections below.

2.1 dS solutions

Since the dS solution corresponds to $c_2 < 0$, it is convenient to characterize the existence of the two horizons by redefining the parameter as follows

$$c_0 = 3\sqrt{3}\frac{\sqrt[3]{-2c_2}}{\beta_m} - \frac{1}{\alpha_g}, \qquad (11)$$

where the condition for having two horizons can be expressed as

$$0 < \beta_m < 1. \qquad (12)$$

Substituting c_1 and c_0 into $f(\tilde{r})$ in Eq. (9), we obtain

$$f_{\text{dS}}(\tilde{r})$$
$$= 1 - \frac{2\tilde{M}}{\tilde{r}} + \alpha_g \left(c_2\tilde{r}^2 - 3\sqrt[3]{4c_2^2}\tilde{r} + 3\sqrt{3}\frac{\sqrt[3]{-2c_2}}{\beta_m} - \frac{1}{\alpha_g} \right). \qquad (13)$$

The horizons can be obtained by solving equation $f_{\text{dS}}(\tilde{r}) = 0$. As a result, such two horizons can be written as

$$\tilde{r}_1 = -\frac{2}{\sqrt[3]{-2c_2}} \left[\sqrt{X} \cos\left(\frac{1}{3}\text{arcsec}(Y) + \frac{\pi}{3} \right) + 1 \right] \qquad (14)$$

and

$$\tilde{r}_2 = \frac{2}{\sqrt[3]{-2c_2}} \left[\sqrt{X} \cos\left(\frac{1}{3}\text{arcsec}(Y) \right) - 1 \right], \qquad (15)$$

where

$$X = \frac{2\sqrt{3}}{\beta_m} + 4 \quad \text{and} \quad Y = -\sqrt{\frac{2}{\beta_m}\frac{(2\beta_m + \sqrt{3})^{3/2}}{5\beta_m + 3\sqrt{3}}}. \qquad (16)$$

From Fig. 1, one can see that the parameter β_m can be used to characterize the existence to two horizons. Moreover, for this setting of parameters, one can find that two horizons in the dRGT black hole are closer than ones in the SdS black hole. This is one of the important properties of the dRGT black hole, which provides a crucial contribution to the greybody factor in the dRGT black hole, which is different from one in the SdS black hole.

2.2 AdS solutions

For the AdS solutions, the parameter c_2 is positive, $c_2 > 0$. By performing in a similar way as done in the dS case, the
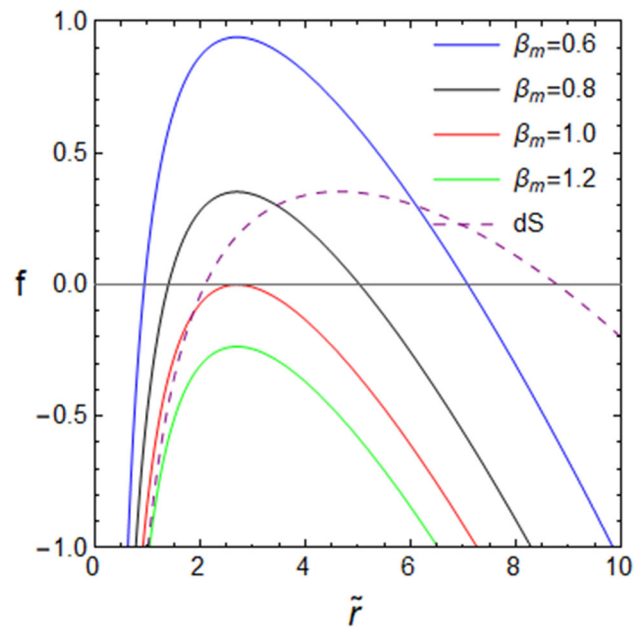
Fig. 1 The plot of $f_{\text{dS}}(\tilde{r})$ with $\tilde{M} = 1$, $c_2 = -0.01$, $\alpha_g = 1$ with various β_m. The dashed purple line represents $f_{\text{SdS}}(\tilde{r})$ ($c_1 = c_0 = 0$)

parameter c_0 can be written in terms of β_m as

$$c_0 = 3\sqrt{3}\frac{\sqrt[3]{2c_2}}{\beta_m} - \frac{1}{\alpha_g}, \qquad (17)$$

where the existence of three horizons can be characterized by parameter β_m as

$$1 < \beta_m < \frac{2}{\sqrt{3}}. \qquad (18)$$

Substituting c_1 and c_0 into $f(\tilde{r})$ in Eq. (9), we obtain

$$f_{\text{AdS}}(\tilde{r})$$
$$= 1 - \frac{2\tilde{M}}{\tilde{r}} + \alpha_g \left(c_2\tilde{r}^2 - 3\sqrt[3]{4c_2^2}\tilde{r} + 3\sqrt{3}\frac{\sqrt[3]{2c_2}}{\beta_m} - \frac{1}{\alpha_g} \right). \qquad (19)$$

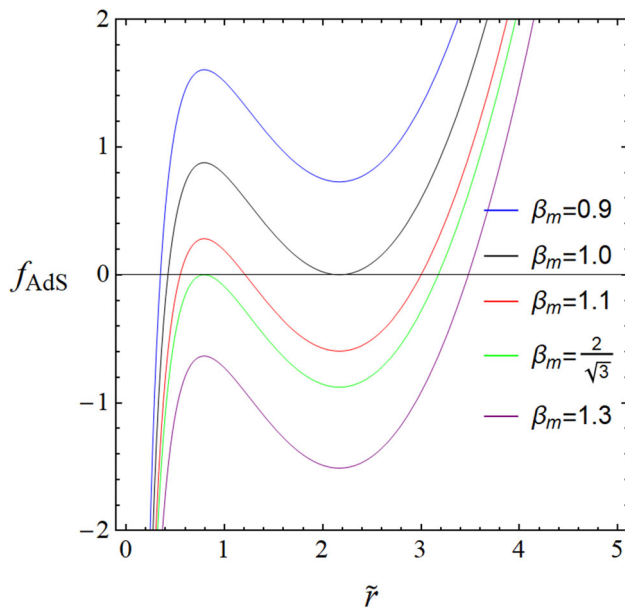By solving $f_{\text{AdS}}(\tilde{r}) = 0$, the three horizons can be expressed as

$$\tilde{r}_1 = \frac{2}{\sqrt[3]{2c_2}} \left[1 - \sqrt{x} \sin\left(\frac{1}{3}\text{arcsec}(y) + \frac{\pi}{6} \right) \right], \qquad (20)$$

$$\tilde{r}_2 = \frac{2}{\sqrt[3]{2c_2}} \left[1 - \sqrt{x} \cos\left(\frac{1}{3}\text{arcsec}(y) + \frac{\pi}{3} \right) \right], \qquad (21)$$

$$\tilde{r}_3 = \frac{2}{\sqrt[3]{2c_2}} \left[1 + \sqrt{x} \cos\left(\frac{1}{3}\text{arcsec}(y) \right) \right], \qquad (22)$$

where

$$x = \frac{4 - 2\sqrt{3}}{\beta_m} \quad \text{and} \quad y = \frac{\sqrt{6} - 2\sqrt{2}\beta_m}{(3\sqrt{3} - 5\beta_m)\sqrt{-\frac{\beta_m}{\sqrt{3} - 2\beta_m}}}. \qquad (23)$$

Fig. 2 The plot of $f(\tilde{r})$ with $\tilde{M} = 1$, $c_2 = 1$, $\alpha_g = 1$ and $\beta_m = 0.9$, 1.0, 1.1, $2/\sqrt{3}$ and 1

From Fig. 2, one can see that the parameter β_m can characterize the existence of three horizons, satisfying the condition in Eq. (18). For $\beta_m = 1$, the second and the third horizons emerge so that in this case, it corresponds to extremal black hole with two horizons. For $\beta_m = 2/\sqrt{3}$, the first and the second horizons emerge. In this case, the black hole is also extremal with two horizons. Note that, for the SAdS black hole, there exists only the first horizon (similar to the case for $\beta_m < 1$). Therefore, the existence of three horizons is a crucial property of the dRGT black hole compared to the SAdS black hole.

Moreover, in order to find the proper form of the potential in the next section, it is worthwhile to find the derivative of the horizon function. As a result, we found that $f'_{\text{dS}}(\tilde{r}) = f'_{\text{AdS}}(\tilde{r})$ and can be written as

$$f'_{\text{dS}}(\tilde{r}) = f'_{\text{AdS}}(\tilde{r}) = \frac{2\tilde{M}}{\tilde{r}^2} + 2\alpha_g c_2 \tilde{r} - 3\alpha_g \sqrt[3]{4c_2^2}. \quad (24)$$

Note that the signs of c_2 are different; for the dS case, c_2 is negative, while for the AdS case, c_2 is positive.

3 Potential of the dRGT black hole

When quantum effects are taken into account, a black hole can emit thermal radiation at its event horizon called the Hawking radiation [1]. This radiation could be any field such as the scalar field or the electromagnetic field. In this work, we are interested in the massive scalar field emitted from a black hole. Its dynamics can be described by the Klein–

Gordon equation on a curved spacetime [41]

$$\frac{1}{\sqrt{-g}} \partial_\mu (\sqrt{-g} g^{\mu\nu} \partial_\nu \Phi) - m^2 \Phi = 0, \quad (25)$$

where $g_{\mu\nu}$ is the metric tensor, $g^{\mu\nu}$ is the inverse of the metric tensor, g is the determinant of the metric tensor and m is the mass of the scalar field.

Since a black hole from Eq. (8) has spherical symmetry, the method of the separation of variables can be used. We write Φ as

$$\Phi(t, r, \theta, \phi) = e^{i\omega t} \frac{\psi(r)}{r} Y_{\ell m}(\theta, \phi), \quad (26)$$

where $Y_{\ell m}(\theta, \phi)$ is a spherical harmonic function. It satisfies

$$\frac{1}{\sin \theta} \frac{\partial}{\partial \theta} \left(\sin \theta \frac{\partial Y_{\ell m}(\theta, \phi)}{\partial \theta} \right) + \frac{1}{\sin^2 \theta} \frac{\partial^2 Y_{\ell m}(\theta, \phi)}{\partial \phi^2}$$
$$= -\ell(\ell + 1) Y_{\ell m}(\theta, \phi), \quad (27)$$

where ℓ is a non-negative integer, m is an integer and $\ell \geq |m|$. The radial part is given by

$$\frac{d^2 \psi(r)}{dr_*^2} + [\omega^2 - V(\tilde{r})] \psi(r) = 0, \quad (28)$$

where

$$\frac{dr_*}{dr} = \frac{1}{|f(\tilde{r})|} \quad (29)$$

and

$$\tilde{V}(\tilde{r}) = f(\tilde{r}) \left[\frac{\ell(\ell + 1)}{\tilde{r}^2} + \frac{f'(\tilde{r})}{\tilde{r}} + \tilde{m}^2 \right]. \quad (30)$$

where $\tilde{V}(\tilde{r}) = c^2 V(\tilde{r})$ and $\tilde{m} = cm$.

3.1 Potentials for the dS case

From Eq. (30), the dS potential is given by

$$\tilde{V}_{\text{dS}}(\tilde{r}) = f_{\text{dS}}(\tilde{r}) \left[\frac{\ell(\ell + 1)}{\tilde{r}^2} + \frac{f'_{\text{dS}}(\tilde{r})}{\tilde{r}} + \tilde{m}^2 \right], \quad (31)$$

where $f_{\text{dS}}(\tilde{r})$ is given in Eq. (13). The potentials for the dS case are plotted for $m = 0$, 0.2 and 0.5, with different β_m in Fig. 3. The graph shows that when m increases, the potential also increases. This is apparent from Eq. (31) which shows that the potential is an increasing function of m because $f_{\text{dS}}(\tilde{r})$ is always positive. Therefore, when m increases, the whole graph is shifted upward as shown in Fig. 3.

For $\ell = 0$, the dS potential for massless scalar field vanishes at $\tilde{r}_{\text{fmax}}$, where $\tilde{r}_{\text{fmax}}$ is the location of the maximum of $f_{\text{dS}}(\tilde{r})$ ($f'_{\text{dS}}(\tilde{r}_{\text{fmax}}) = 0$). However, for the massive scalar field, it does not vanish at this point, but is still positive and vanishes at $\tilde{r} > \tilde{r}_{\text{fmax}}$. We can see this from Fig. 3 that the $\tilde{r}$ intercept of the red curve ($m = 0.5$) is on the right of that of the blue curve ($m = 0$). Thus, the mass of the scalar field has effects on the area under the curve of the potential. The

(a)

(b)
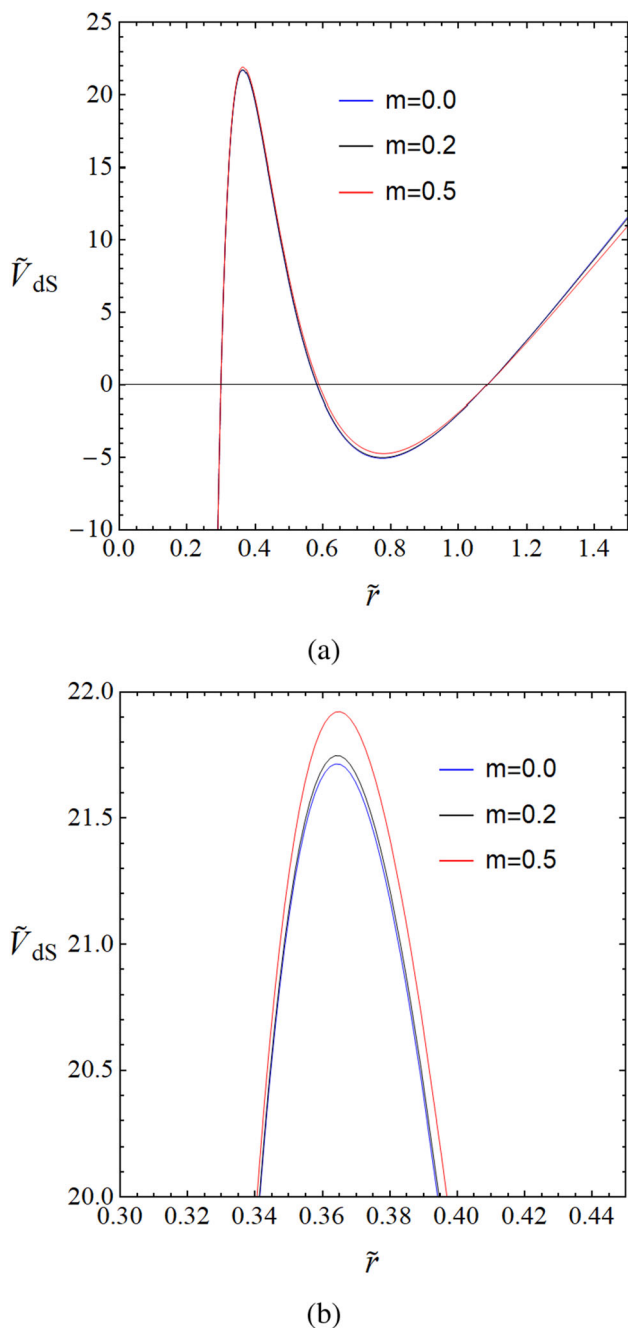
Fig. 3 a The dRGT potentials for the dS case with $\ell = 0, \tilde{M} = 1, c_2 = -1, \alpha_g = 1, \beta_m = 0.8$ and $m = 0, 0.2$ and 0.5. **b** The magnification of **a**

scalar mass increases the area which is above the $\tilde{r}$ axis, and decrease the area which is below the $\tilde{r}$ axis.

The dS potentials are plotted with different β_m and c_2 in Fig. 4a, b, respectively. From Fig. 4a, we see that when β_m increases, the local maximum of the potential decreases, while the local minimum increases. This can be seen by finding the derivative of the potential in Eq. (31) with respect to β_m

$$\frac{d\tilde{V}_{dS}}{d\beta_m} = -3\sqrt{3}\alpha_g \frac{\sqrt[3]{-2c_2}}{\beta_m^2} \left[\frac{\ell(\ell+1)}{\tilde{r}^2} + \frac{f'_{dS}(\tilde{r})}{\tilde{r}} + \tilde{m}^2 \right]. \quad (32)$$

If the sum of all terms in the square bracket is positive, we obtain $d\tilde{V}_{dS}/d\beta_m < 0$, and the potential decreases with increasing β_m. On the other hand, if the sum of all terms in the square bracket is negative, the potential increases with increasing β_m. Since $f_{dS}(\tilde{r})$ is always positive, from Eq. (31), the potential has the same sign as the square bracket term. Therefore, when the potential is positive, corresponding to the positive square bracket term, it decreases with increasing β_m. We can see from Fig. 4a that the red curve ($\beta_m = 0.9$) is below the blue curve ($\beta_m = 0.8$) in the region where the potential is positive. Conversely, when the potential is negative, corresponding to the negative square bracket term, it increases with increasing β_m. Again, we can see from Fig. 4a that the red curve ($\beta_m = 0.9$) is above the blue curve ($\beta_m = 0.8$) in the region where the potential is negative. Moreover, when β_m increases, the width of the potential decreases.

For Fig. 4b, we see that when c_2 decreases, the local maximum of the potential increases, while the local minimum decreases. Since c_2 represents the negative of the cosmological constant, the decrease in c_2 for the dS case corresponds to the increase in the magnitude of the positive cosmological constant. Therefore, the graph shows that the local maximum of the potential increases when the magnitude of the cosmological constant increases.

When $c_1 = c_0 = 0$, the asymptotically dS spacetime in the dRGT massive gravity reduces to the Schwarzschild de Sitter (SdS) spacetime. The function $f(\tilde{r})$ of the SdS spacetime can be obtained by letting $c_1 = c_0 = 0$ in Eq. (9)

$$f_{SdS}(\tilde{r}) = 1 - \frac{2\tilde{M}}{\tilde{r}} + \alpha_g c_2 \tilde{r}^2 \quad (33)$$

and c_2 be negative. Then, from Eq. (30), the SdS potential is given by

$$\tilde{V}_{SdS}(\tilde{r}) = f_{SdS}(\tilde{r}) \left[\frac{\ell(\ell+1)}{\tilde{r}^2} + \frac{f'_{SdS}(\tilde{r})}{\tilde{r}} + \tilde{m}^2 \right]. \quad (34)$$

The potentials for an SdS black hole and an asymptotically dS black hole in the dRGT massive gravity are plotted in Fig. 5. We see that the potential for the dS black hole in the dRGT massive gravity (the solid curve) is shifted left from the potential for the SdS black hole (the dashed curve). The massive gravity shrinks the horizons of a black hole, which is apparent from Fig. 1. Notice that when m increases, the absolute area of the dS potential for $\ell = 0$ in the negative region decreases. This means that if m continues to increase to some value, called m_{min}, the dS potential becomes positive on the interval $\tilde{r}_1 < \tilde{r} < \tilde{r}_2$. To find m_{min}, we rewrite Eq. (31) for $\ell = 0$ as

$$\tilde{V}_{dS,\ell=0}(\tilde{r})$$

(a)

(b)
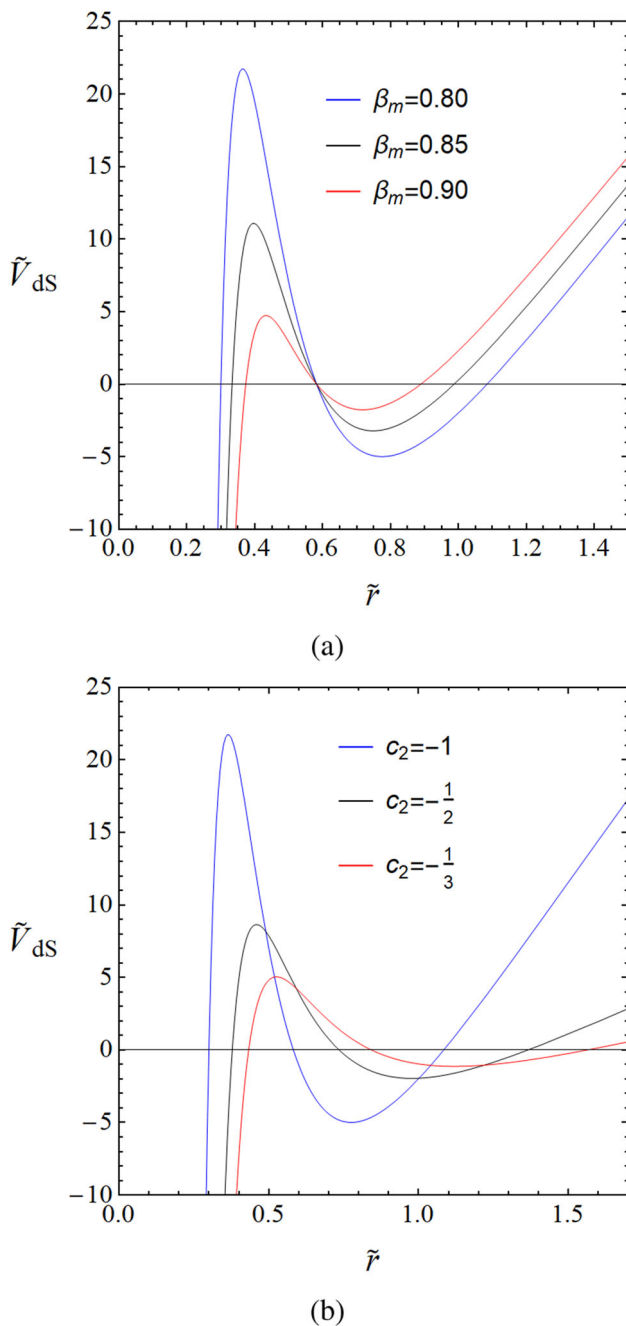
Fig. 4 The dRGT potentials for the dS case with $\ell = 0$, $\tilde{M} = 1$, $\alpha_g = 1$, and $m = 0.2$. **a** $c_2 = -1$ and $\beta_m = 0.8$, 0.85 and 0.9. **b** $\beta_m = 0.8$ and $c_2 = -1$, $-1/2$ and $-1/3$

$$= f_{\text{dS}}(\tilde{r}) \left(\frac{2\tilde{M}}{\tilde{r}^3} + 2\alpha_g c_2 - \frac{3\alpha_g \sqrt[3]{4c_2^2}}{\tilde{r}} + \tilde{m}^2 \right).$$
(35)

It is positive for $\tilde{r}_1 < \tilde{r} < \tilde{r}_2$ if

$$\tilde{m}^2 > -\frac{2\tilde{M}}{\tilde{r}^3} - 2\alpha_g c_2 + \frac{3\alpha_g \sqrt[3]{4c_2^2}}{\tilde{r}}.$$
(36)

We define $\tilde{m}_{\min}$ as

$$\tilde{m}_{\min}^2 = \max \left[-\frac{2\tilde{M}}{\tilde{r}^3} - 2\alpha_g c_2 + \frac{3\alpha_g \sqrt[3]{4c_2^2}}{\tilde{r}} \right],$$
(37)

where $\tilde{r}_1 < \tilde{r} < \tilde{r}_2$. We find that the maximum is at $\tilde{r} = \tilde{r}_2$. Therefore,

$$\tilde{m}_{\min}^2 = -\frac{2\tilde{M}}{\tilde{r}_2^3} - 2\alpha_g c_2 + \frac{3\alpha_g \sqrt[3]{4c_2^2}}{\tilde{r}_2}.$$
(38)

For $\tilde{M} = 1$, $c_2 = -0.01$ and $\alpha_g = 1$, we obtain

$$\tilde{m}_{\min}^2 = 0.02 + \frac{0.22}{\tilde{r}_2} - \frac{2}{\tilde{r}_2^3}.$$
(39)

For $\beta_m = 0.875$ and $c_2 = -0.01$, we obtain $\tilde{r}_2 = 4.357$. Therefore,

$$\tilde{m}_{\min} = 0.215.$$
(40)

Moreover, when $\tilde{m} = 0.2$, an SdS potential for $\ell = 0$ is positive on the interval $\tilde{r}_1 < \tilde{r} < \tilde{r}_2$. In the case of the SdS black hole, $\tilde{m}_{\min}$ in Eq. (38) reduces to

$$\tilde{m}_{\min}^2 = -\frac{2\tilde{M}}{\tilde{r}_2^3} - 2\alpha_g c_2.$$
(41)

For $c_2 = -0.01$ and $\beta_m = 0.875$, which give $\tilde{r}_2 = 8.79$, and $\tilde{M} = 1$ and $\alpha_g = 1$, we obtain

$$\tilde{m}_{\min} = 0.13.$$
(42)

This is why the SdS potential for $\ell = 0$ in Fig. 5 is positive for $\tilde{r}_1 < \tilde{r} < \tilde{r}_2$ at $\tilde{m} = 0.2$.

Furthermore, for $\ell = 1$, the potentials are positive for $\tilde{r}_1 < \tilde{r} < \tilde{r}_2$. To see this, we rewrite Eq. (31) as

$$\tilde{V}_{\text{dS}}(\tilde{r})$$
$$= f_{\text{dS}}(\tilde{r}) \left[\frac{\ell(\ell+1)}{\tilde{r}^2} + \frac{2\tilde{M}}{\tilde{r}^3} + 2\alpha_g c_2 - \frac{3\alpha_g \sqrt[3]{4c_2^2}}{\tilde{r}} + \tilde{m}^2 \right].$$
(43)

It is positive for $\tilde{r}_1 < \tilde{r} < \tilde{r}_2$ if

$$\ell(\ell+1) > -\frac{2\tilde{M}}{\tilde{r}} - 2\alpha_g c_2 \tilde{r}^2 + 3\alpha_g \sqrt[3]{4c_2^2}\tilde{r} - \tilde{m}^2 \tilde{r}^2.$$
(44)

From this expression, the left hand side is in the order of unity and the right hand side is typically less than unity by the requirement of the existence of the horizons. For example, for a typical scale of the existence of the horizons, $c_2 \sim -0.01$ and then $\tilde{r} \gtrsim 1$. For the usual scale of the scalar mass $\tilde{m}^2 \sim 0.01$, the second term and the forth term are in the same order, which provide a tiny contribution. The third term is in the order of $0.1\tilde{r}$ which contributes to the same order as the first term in the opposite sign. Therefore, the amount of contribution of the right hand side is usually smaller than
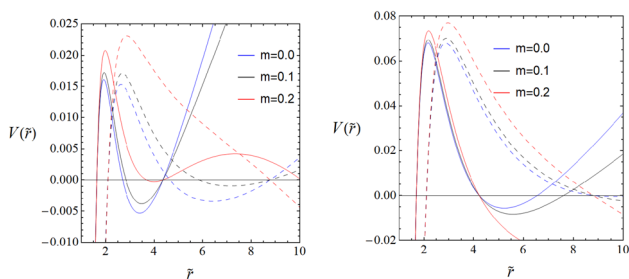
Fig. 5 The potentials with ($\ell = 0$ left panel and $\ell = 1$ right panel), $\tilde{M} = 1$, $c_2 = -0.01$, $\alpha_g = 1$. The solid lines represent the potential for an asymptotically dS black hole in dRGT massive gravity ($\beta_m = 0.875$ for left panel and $\beta_m = 0.89$ for right panel). The dashed lines represent the potential for an SdS black hole ($c_1 = c_0 = 0$)

unity. For example, by setting $\tilde{M} = \alpha_g = 1$, $c_2 = -0.01$, $\beta_m = 0.875$ and $\tilde{r} \sim \tilde{r}_2 \sim 4.36$, we obtain $\ell(\ell+1) > 0.0034$ with $m^2 = 0.05$. As a result, one can see that it is difficult to obtain the negative part of the potential for the case of $\ell \geq 1$.

3.2 Potentials of the AdS case

From Eq. (30), the AdS potential is given by

$$\tilde{V}_{\text{AdS}}(\tilde{r}) = f_{\text{AdS}}(\tilde{r}) \left[\frac{\ell(\ell+1)}{\tilde{r}^2} + \frac{f'_{\text{AdS}}(\tilde{r})}{\tilde{r}} + \tilde{m}^2 \right], \quad (45)$$

where $f_{\text{AdS}}(\tilde{r})$ is given in Eq. (19). In the AdS case, $f_{\text{AdS}}(\tilde{r})$ has three horizons. Thus, from Eq. (45), the potential is zero at five points of $\tilde{r}$.

The AdS potentials are plotted in Fig. 6. Consider the effect of m. Different from the dS case, the AdS potential is an increasing function in m when $f_{\text{AdS}}(\tilde{r}) > 0$ and a decreasing function in m when $f_{\text{AdS}}(\tilde{r}) < 0$. In the range $\tilde{r}_1 < \tilde{r} < \tilde{r}_2$, where $f_{\text{AdS}}(\tilde{r})$ is positive, the graph is shifted upward with increasing m. On the other hand, in the range $\tilde{r}_2 < \tilde{r} < \tilde{r}_3$, where $f_{\text{AdS}}(\tilde{r})$ is negative, the graph is shifted downward with increasing m. These are shown in Fig. 6 where we can see the red curve ($m = 0.5$) is above the blue curve ($m = 0$) in the range $\tilde{r}_1 < \tilde{r} < \tilde{r}_2$, while the red curve is below the blue curve in the range $\tilde{r}_2 < \tilde{r} < \tilde{r}_3$. The mass of scalar field can increase or decrease the potential depending on the sign of $f_{\text{AdS}}(\tilde{r})$.

The AdS potentials are plotted with different β_m and c_2 in Fig. 7a, b, respectively. We can analyze the effects of β_m on the potential by finding the derivative of the potential in Eq. (45) with respect to β_m

$$\frac{d\tilde{V}_{\text{AdS}}}{d\beta_m} = -3\sqrt{3}\alpha_g \frac{\sqrt[3]{2c_2}}{\beta_m^2} \left[\frac{\ell(\ell+1)}{\tilde{r}^2} + \frac{f'_{\text{AdS}}(\tilde{r})}{\tilde{r}} + \tilde{m}^2 \right]. \quad (46)$$

Similar to the dS case, if the square bracket term is positive, the potential decreases with increasing β_m. On the other hand, if the square bracket term is negative, the potential increases
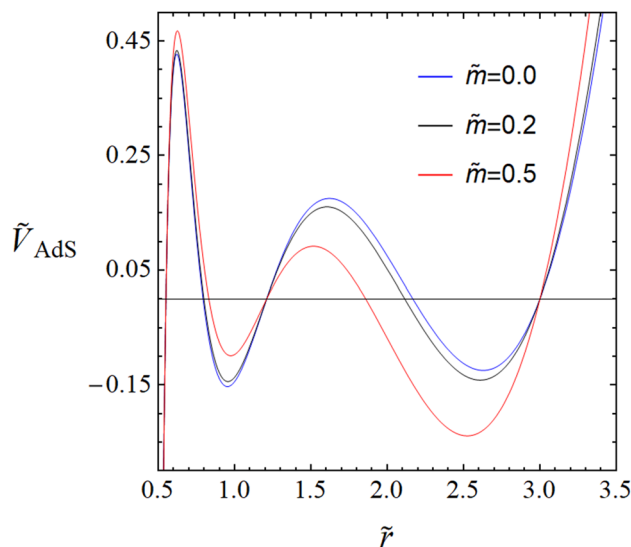
Fig. 6 The AdS potentials with $\ell = 0$, $\tilde{M} = 1$, $c_2 = 1$, $\alpha_g = 1$, $\beta_m = 1.1$ and $\tilde{m} = 0$, 0.2 and 0.5

with increasing β_m. In the range $\tilde{r}_1 < \tilde{r} < \tilde{r}_{\text{max}1}$, the square bracket term is positive. Therefore, the potential in this range decreases with increasing β_m. We can see from Fig. 7a that the red curve ($\beta_m = 1.12$) is below the blue curve ($\beta_m = 1.08$). In the range $\tilde{r}_{\text{max}1} < \tilde{r} < \tilde{r}_2$, the square bracket term is negative. Thus, the potential in this range increases with increasing β_m. We can see that the red curve is above the blue curve. In the range $\tilde{r}_2 < \tilde{r} < \tilde{r}_{\text{max}2}$, the square bracket term is again negative. Then, the potential in this range increases with increasing β_m. We can see that the red curve is above the blue curve. In the range $\tilde{r}_{\text{max}2} < \tilde{r} < \tilde{r}_3$, the square bracket term is positive and the potential in this range decreases with increasing β_m. We can see that the red curve is below the blue curve.

For Fig. 7b, we see that when c_2 increases, the relative maximum of the potential also increases. The increase in c_2 for the AdS case corresponds to the increase in the magnitude of the negative cosmological constant. Therefore, the graph shows that the local maximum of the potential increases when the magnitude of the cosmological constant increases.

The AdS potentials for $\ell = 2$ are plotted in Fig. 8. We see that the potentials are positive on $\tilde{r}_1 < \tilde{r} < \tilde{r}_2$ and negative on $\tilde{r}_2 < \tilde{r} < \tilde{r}_3$.

4 Greybody factors of black holes

When quantum effects are taken into account, a black hole can emit thermal radiation as a blackbody spectrum at its event horizon called the Hawking radiation [1]. While propagating away from the black hole, the Hawking radiation encounters the black hole spacetime curvature, which modi-

(a)

(b)
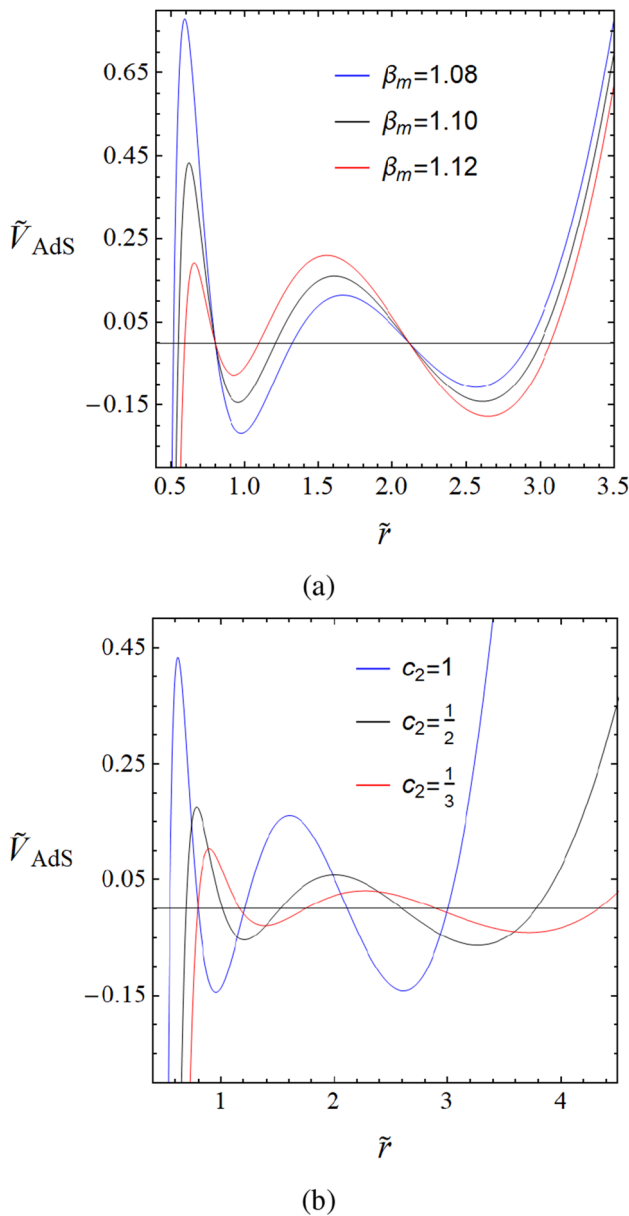
Fig. 7 The AdS potentials with $\ell = 0$, $\tilde{M} = 1$, $\alpha_g = 1$, and $\tilde{m} = 0.2$. **a** $c_2 = 1$ and $\beta_m = 1.08$, 1.10 and 1.12. **b** $\beta_m = 1.1$ and $c_2 = 1$, $1/2$ and $1/3$

fies it. Therefore, an observer at a distant no longer sees the blackbody spectrum. Rather, he measures a modified one, which is called greybody. A quantity that measures how much the modified spectrum deviates from the blackbody spectrum is called the greybody factor. From a black hole scattering point of view, a black hole spacetime curvature acts as a potential barrier. The greybody factor is defined as a transmission coefficient.

There are various methods to compute the greybody factor. One of them is to find its lower bound rather than its exact
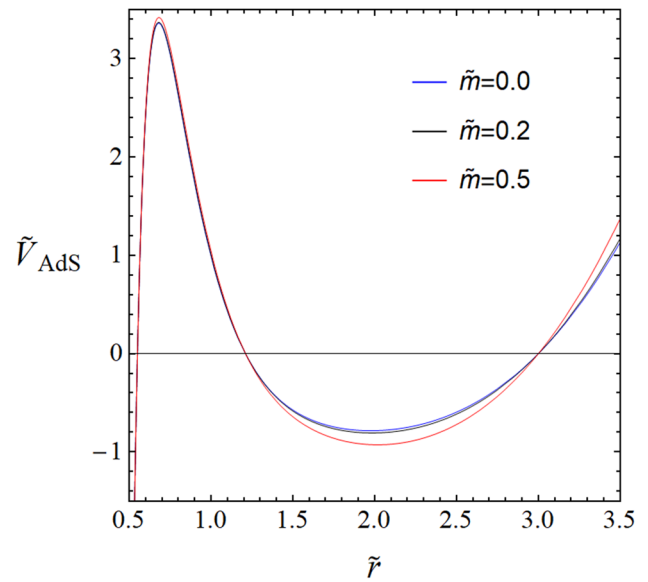
Fig. 8 The AdS potentials with $c_2 = 1$, $\beta_m = 1.1$, $\tilde{M} = 1$, $\alpha_g = 1$, $\tilde{m} = 0$, 0.2 and 0.5 and $\ell = 2$

value. The bounds of the greybody factors are given by [2,4]

$$T \geq \text{sech}^2 \left[\int_{-\infty}^{\infty} \vartheta \, dr_* \right], \tag{47}$$

where

$$\vartheta \equiv \frac{\sqrt{[h'(r_*)]^2 + [\omega^2 - V(\tilde{r}) - h^2(r_*)]^2}}{2h(r_*)}, \tag{48}$$

for some positive function h satisfying $h(-\infty) = \sqrt{\omega^2 - V_{-\infty}}$ and $h(\infty) = \sqrt{\omega^2 - V_{\infty}}$, where $V_{\pm\infty} = V(\pm\infty)$. For a potential satisfying $V_{\pm\infty} = 0$, we can set $h = \omega$, then

$$T \geq \text{sech}^2 \left[\frac{1}{2\omega} \int_{-\infty}^{\infty} |V(\tilde{r})| \, dr_* \right]. \tag{49}$$

From Eq. (29) and $\tilde{r} = r/c$, we obtain

$$T \geq \text{sech}^2 \left[\frac{1}{2\tilde{\omega}} \int_{\tilde{r}_1}^{\tilde{r}_2} |\tilde{V}(\tilde{r})| \frac{1}{|f(\tilde{r})|} \, d\tilde{r} \right], \tag{50}$$

where $\tilde{\omega} = \omega c$. From the triangle inequality,

$$\left| \int_a^b f(x) dx \right| \leq \int_a^b |f(x)| dx, \tag{51}$$

we obtain

$$\text{sech} \left(\int_a^b f(x) dx \right) \geq \text{sech} \left(\int_a^b |f(x)| dx \right), \tag{52}$$

which follows from

$$\text{sech}(|x|) = \text{sech}(x). \tag{53}$$

Then,

$$\text{sech}^2\left(\int_a^b f(x)dx\right) \geq \text{sech}^2\left(\int_a^b |f(x)|dx\right). \quad (54)$$

From Eq. (50), we define

$$T_{\text{app}} \equiv \text{sech}^2\left[\frac{1}{2\tilde{\omega}}\int_{\tilde{r}_1}^{\tilde{r}_2}\frac{\tilde{V}(\tilde{r})}{f(\tilde{r})}d\tilde{r}\right] \quad (55)$$

and

$$T_{\text{b}} \equiv \text{sech}^2\left[\frac{1}{2\tilde{\omega}}\int_{\tilde{r}_1}^{\tilde{r}_2}|\tilde{V}(\tilde{r})|\frac{1}{|f(\tilde{r})|}d\tilde{r}\right]. \quad (56)$$

From Eq. (54), we obtain

$$T_{\text{app}} \geq T_{\text{b}}. \quad (57)$$

We can rewrite Eq. (50) as

$$T \geq T_{\text{b}}. \quad (58)$$

If $T \geq T_{\text{app}}$, we may say that T_{app} is a better bound than T_{b}. If $T_{\text{app}} \geq T$, we cannot conclude which one, T_{app} or T_{b}, is a better bound.

It is worthwhile to note that the calculation of the greybody factor by using the rigorous bound can provide us with a useful way to analyze the behaviour qualitatively, since it is possible to find the explicit expression for the greybody factor. However, since it is the bound, it may not provide the approximated value of the greybody factor. For example, in the high ℓ case, the bound is much lower than the approximated value. In this case, it is more convenient to use other methods to calculate the bound. In this paper, we choose to investigate the greybody factor by using the third order of the WKB approximation proposed by Iyer and Will [43]. This is a well-developed method to study the barrier-like Quasinormal modes and the greybody factor.

For the WKB approximation, it is convenient to rewrite the redial equation in Eq. (3) in the form as

$$\left(\frac{d^2}{dr_*^2} + Q\right)\psi = 0, \quad (59)$$

where $Q = \omega^2 - V$. Moreover, we also use the approximation as $\omega^2 \approx V_{\text{max}}$, where V_{max} denotes the maximum value of the effective potential. The greybody factor for this approximation is given by [44]

$$T = \frac{1}{1 + \exp^{2S(\omega)}}. \quad (60)$$

The function $S(\omega)$ can be expressed as

$$S(\omega) = \pi k^{1/2}\left[\frac{1}{2}z_0^2 + \left(\frac{15}{64}b_3^2 - \frac{3}{16}b_4\right)z_0^4\right]$$
$$+ \pi k^{-1/2}\left[\frac{3}{16}b_4 - \frac{7}{64}b_3^2\right]$$

$$+ \pi k^{1/2}\left[\frac{1155}{2048}b_3^4 - \frac{315}{256}b_3^2 b_4 + \frac{35}{128}b_4^2\right.$$
$$\left. + \frac{35}{64}b_3 b_5 - \frac{5}{32}b_6\right]z_0^6$$
$$- \pi k^{-1/2}\left[\frac{1365}{2048}b_3^4 - \frac{525}{256}b_3^2 b_4 + \frac{85}{128}b_4^2\right.$$
$$\left. + \frac{95}{64}b_3 b_5 - \frac{25}{32}b_6\right]z_0^2 + O(\omega), \quad (61)$$

where $O(\omega)$ is a set of the higher order terms and

$$z_0^2 = -\frac{Q_{\text{max}}}{k}$$
$$k = \frac{1}{2}\left(\frac{d^2 Q}{dr_*^2}\right)_{\text{max}} \quad (62)$$
$$b_n = \left(\frac{1}{n!k}\right)\left(\frac{d^n Q}{dr_*^n}\right)_{\text{max}}.$$

Note that the subscript "max" denotes the quantities for $r = r_{\text{max}}$ after taking the derivative where r_{max} denotes the position of V_{max}. In this way, one can find the greybody factor by using the numerical method. Note that the results evaluated by using the WKB method cannot be done for low multipole, especially for $\ell = 0$. In this case, we cannot compare the results between such two methods.

4.1 Greybody factors for the dS case

A dS black hole has two horizons; namely, event horizon and the cosmological horizon. Its potential is shown in Fig. 5. It can be seen that the dS potential for $\ell = 0$ with $\tilde{m} < \tilde{m}_{\text{min}}$ can be both positive and negative, while one for $\ell = 0$ with $\tilde{m} > \tilde{m}_{\text{min}}$ and $\ell = 1$ is always positive. Therefore, finding the bounds on the greybody factors for such two cases can be done independently.

4.1.1 $\ell = 0$ and $\tilde{m} < \tilde{m}_{\text{min}}$

For $\ell = 0$, the dS potential is positive for $\tilde{r}_1 < \tilde{r} < \tilde{r}_{\text{cri}}$ and negative for $\tilde{r}_{\text{cri}} < \tilde{r} < \tilde{r}_2$, while $f_{\text{dS}}(\tilde{r})$ is always positive for $\tilde{r}_1 < \tilde{r} < \tilde{r}_2$, where $\tilde{r}_{\text{cri}}$ is the point satisfying $f'_{\text{dS}}(\tilde{r}_{\text{cri}}) = -\tilde{m}^2 \tilde{r}_{\text{cri}}$. We can write

$$T_{\text{dS},\ell=0} \geq T_{\text{b, dS},\ell=0}, \quad (63)$$

where

$$T_{\text{b, dS},\ell=0} = \text{sech}^2\left[\frac{1}{2\tilde{\omega}}\int_{\tilde{r}_1}^{\tilde{r}_{\text{cri}}}\frac{\tilde{V}_{\text{dS},\ell=0}(\tilde{r})}{f_{\text{dS}}(\tilde{r})}d\tilde{r}\right.$$
$$\left. - \frac{1}{2\tilde{\omega}}\int_{\tilde{r}_{\text{cri}}}^{\tilde{r}_2}\frac{\tilde{V}_{\text{dS},\ell=0}(\tilde{r})}{f_{\text{dS}}(\tilde{r})}d\tilde{r}\right] \quad (64)$$

and, from Eq. (31), $\tilde{V}_{dS,\ell=0}(\tilde{r})/f_{dS}(\tilde{r})$ is given by

$$\frac{\tilde{V}_{dS,\ell=0}(\tilde{r})}{f_{dS}(\tilde{r})} = \frac{2\tilde{M}}{\tilde{r}^3} + 2\alpha_g c_2 - \frac{3\alpha_g \sqrt[3]{4c_2^2}}{\tilde{r}} + \tilde{m}^2. \tag{65}$$

Calculating the integrals, we obtain

$$
\begin{aligned}
T_{b,\,dS,\ell=0} = \operatorname{sech}^2 & \left[\frac{1}{2\tilde{\omega}} \left\{ \tilde{M} \left(\frac{1}{\tilde{r}_1^2} + \frac{1}{\tilde{r}_2^2} - \frac{2}{\tilde{r}_{cri}^2} \right) \right. \right. \\
& \left. - 2\alpha_g c_2(\tilde{r}_1 + \tilde{r}_2 - 2\tilde{r}_{cri}) - 3\alpha_g \sqrt[3]{4c_2^2} \ln \frac{\tilde{r}_{cri}^2}{\tilde{r}_1 \tilde{r}_2} \right. \\
& \left. \left. - \tilde{m}^2(\tilde{r}_1 + \tilde{r}_2 - 2\tilde{r}_{cri}) \right\} \right].
\end{aligned} \tag{66}
$$

Since the bound of the greybody factor depends on the integral of $\tilde{V}/f$, it can be analyzed by determining the absolute area under the graph of $\tilde{V}/f$. In this case, there exists the negative part of $\tilde{V}/f$, so that it is possible to minimize the area by choosing the proper value of $\tilde{m}$. This corresponds to the maximized greybody factor bound T_b. In fact, one can find $\tilde{r}$ in terms of $\tilde{m}$ from $\tilde{V}/f|_{\tilde{r}=\tilde{r}_{cri}} = 0$. We can find the integral of $\tilde{V}/f$, which depends on $\tilde{r}_{cri}$. Therefore, in principle, one can find the integral, which is a function of $\tilde{m}$. Then, we can find the critical mass $\tilde{m}_c$ to minimize the integral corresponding to the maximized T_b. The expression is very lengthy, we do not express it here. For $c_2 = -0.01$, $\beta_m = 0.875$, the critical mass can be evaluated as $\tilde{m}_c \sim 0.14$. This behaviour of the bounds on the greybody factors is shown in Fig. 9. From Fig. 9a, we see that the bound on the greybody factors increases with increasing $\tilde{m}$ for $0 \le \tilde{m} \le 0.14$. For $\tilde{m} > 0.14$ the bound starts to decrease with increasing $\tilde{m}$. This can be inferred from Fig. 9b that the absolute of the area under the graph on an interval $\tilde{r}_1 < \tilde{r} < \tilde{r}_{cri}$ increases with increasing $\tilde{m}$ and that on an interval $\tilde{r}_{cri} < \tilde{r} < \tilde{r}_2$ decreases with increasing $\tilde{m}$. As a result, there exists a critical mass of the scalar field, which provides the maximum bound of the greybody factor. This is a crucial behaviour of the scalar field mass on the greybody factor.

The bounds on the greybody factors with different β_m and c_2 are plotted in Fig. 10a, b, respectively. For Fig. 10a, we see that when β_m increases, the dS bound on the greybody factors also increases. This follows from Fig. 4a where the local maximum of the potential decreases with increasing β_m.

For Fig. 10b, we see that when c_2 decreases, corresponding to the increase in the magnitude of the positive cosmological constant, the bound on the greybody factors also decreases. This follows from Fig. 4b where the local maximum of the potential increases with the increase in the absolute value of c_2. In the background with the stronger cosmological constant, the massive scalar field can penetrate the dS potential, but with more difficulty.
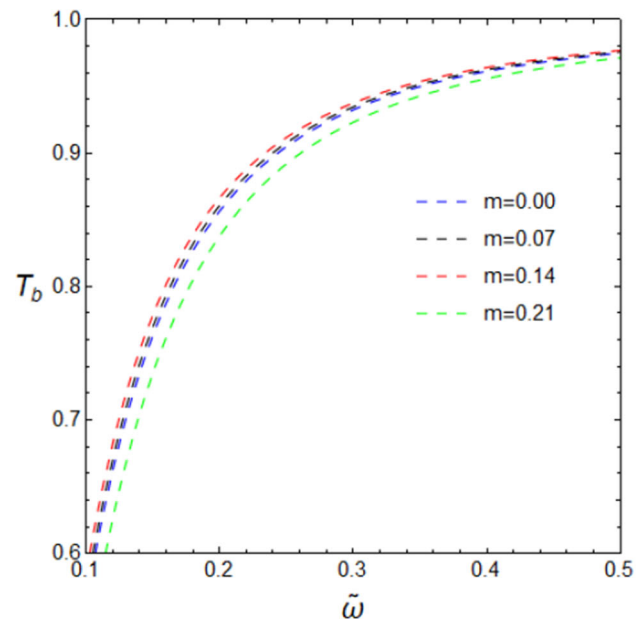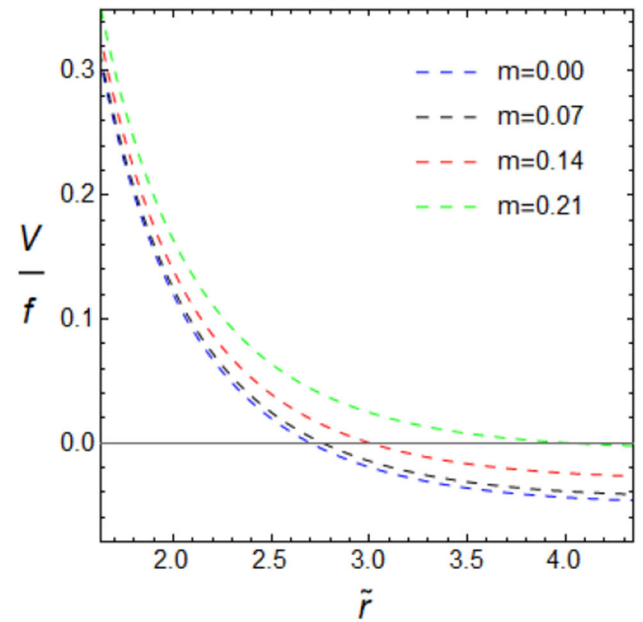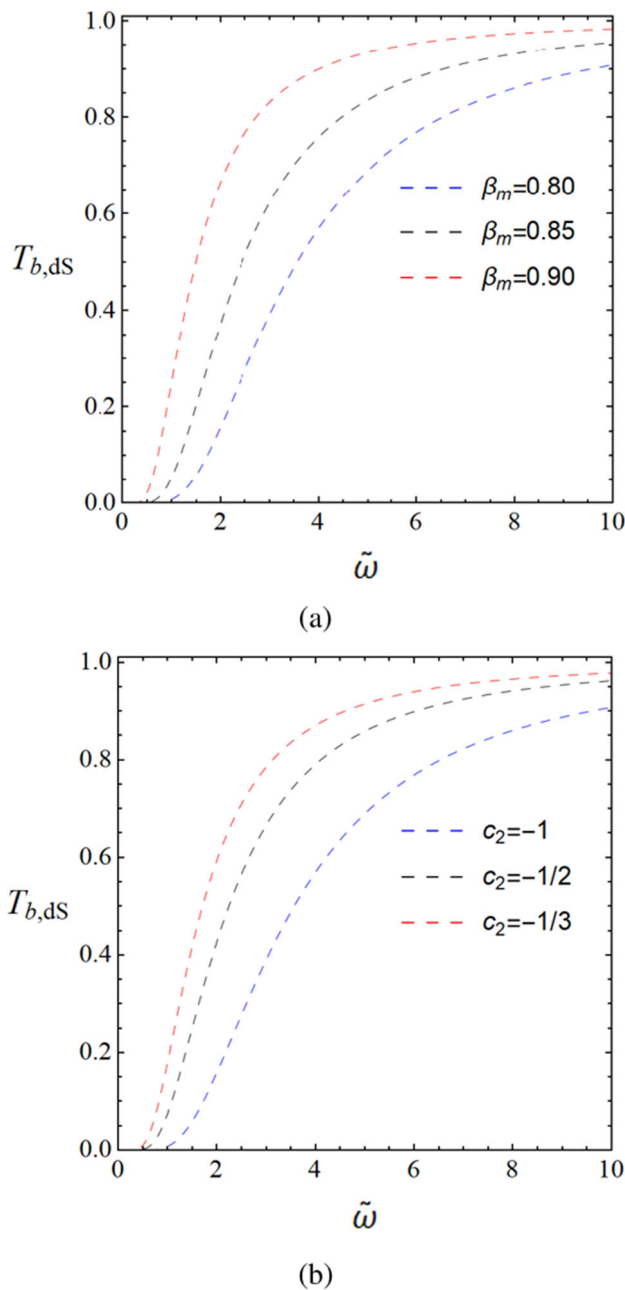

Fig. 9 **a** The rigorous bounds on the greybody factors in the dS case with $\ell = 0$, $\tilde{M} = 1$, $\alpha_g = 1$, $c_2 = -0.01$, $\beta_m = 0.875$ and $\tilde{m} = 0$, 0.07, 0.14 and 0.21. **b** The graph of the function $\tilde{V}/f$ in the dS case with the same parameters

The graphs of T_{app} with different $\tilde{m}$, β_m and c_2 are plotted in Fig. 11a–c, respectively. From Fig. 11a, we see that when $\tilde{m}$ increases, the bound on the greybody factors decreases because the result follows from the dS potential in Fig. 3, which increases with increasing $\tilde{m}$. The more massive the

Fig. 10 The rigorous bounds on the greybody factors in the dS case with $\ell = 0$, $\tilde{M} = 1$, $\alpha_g = 1$. **a** $c_2 = -1$, $\tilde{m} = 0.2$ and $\beta_m = 0.8, 0.85$ and 0.9. **b** $\tilde{m} = 0.2$, $\beta_m = 0.8$ and $c_2 = -1, -1/2$ and $-1/3$

scalar field, it can be harder to transmit out from the dS potential.

For Fig. 11b, we see that when β_m increases, the dS bound on the greybody factors also increases. This follows from Fig. 4a where the local maximum of the potential decreases with increasing β_m.

For Fig. 11c, we see that when c_2 decreases, corresponding to increase in the magnitude of the positive cosmological constant, the bound on the greybody factors also decreases.

This follows from Fig. 4b where the local maximum of the potential increases with decreasing c_2. In the background with the stronger cosmological constant, the massive scalar field can penetrate the dS potential, but with more difficulty.

Moreover, we explicitly see that T_{app} (the solid curve) is greater than or equal to T_b (the dash curve) according to the inequality (57).

4.1.2 $\ell = 0$ with $\tilde{m} > \tilde{m}_{\min}$ and $\ell = 1$

From Fig. 5, the potential for $\ell = 0$ with $\tilde{m} > \tilde{m}_{\min}$ and $\ell = 1$ is positive on the interval $\tilde{r}_1 < \tilde{r} < \tilde{r}_2$. Therefore, from Eqs. (55) and (56), $T_b = T_{\text{app}}$. Then, Eq. (58) becomes

$$T_{\text{dS}} \geq T_{b,\text{dS}}, \tag{67}$$

where

$$T_{b,\text{dS}} = \text{sech}^2 \left[\frac{1}{2\tilde{\omega}} \int_{\tilde{r}_1}^{\tilde{r}_2} \frac{\tilde{V}_{\text{dS}}(\tilde{r})}{f_{\text{dS}}(\tilde{r})} d\tilde{r} \right] \tag{68}$$

and

$$\frac{\tilde{V}_{\text{dS}}(\tilde{r})}{f_{\text{dS}}(\tilde{r})} = \frac{\ell(\ell+1)}{\tilde{r}^2} + \frac{2\tilde{M}}{\tilde{r}^3} + 2\alpha_g c_2 - \frac{3\alpha_g \sqrt[3]{4c_2^2}}{\tilde{r}} + \tilde{m}^2. \tag{69}$$

Calculating the integrals, we obtain

$$T_{b,\text{dS}} = \text{sech}^2 \left[\frac{1}{2\tilde{\omega}} \left\{ \ell(\ell+1) \left(\frac{1}{\tilde{r}_1} - \frac{1}{\tilde{r}_2} \right) \right. \right.$$
$$+ \tilde{M} \left(\frac{1}{\tilde{r}_1^2} - \frac{1}{\tilde{r}_2^2} \right) + 2\alpha_g c_2 (\tilde{r}_2 - \tilde{r}_1)$$
$$\left. \left. - 3\alpha_g \sqrt[3]{4c_2^2} \ln \frac{\tilde{r}_2}{\tilde{r}_1} + \tilde{m}^2 (\tilde{r}_2 - \tilde{r}_1) \right\} \right]. \tag{70}$$

For SdS black holes, the logarithmic term disappears and the above bound reduces to

$$T_{b,\text{SdS}} = \text{sech}^2 \left[\frac{1}{2\tilde{\omega}} \left\{ \ell(\ell+1) \left(\frac{1}{\tilde{r}_1} - \frac{1}{\tilde{r}_2} \right) \right. \right.$$
$$+ \tilde{M} \left(\frac{1}{\tilde{r}_1^2} - \frac{1}{\tilde{r}_2^2} \right) + 2\alpha_g c_2 (\tilde{r}_2 - \tilde{r}_1)$$
$$\left. \left. + \tilde{m}^2 (\tilde{r}_2 - \tilde{r}_1) \right\} \right]. \tag{71}$$
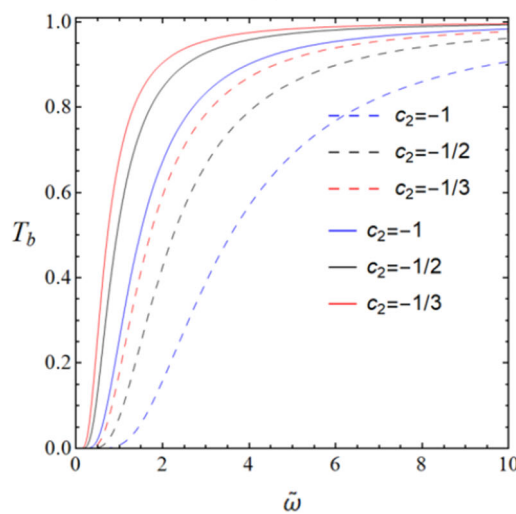
The bounds on the greybody factors of the SdS black holes and the asymptotically dS black holes in the dRGT massive gravity are plotted in Fig. 12. We see that the bounds of the SdS black holes are lower than ones of the asymptotically dS black holes in the dRGT massive gravity. This follows from the fact that the logarithmic term in Eq. (70) is negative. Therefore, $T_{b,\text{SdS}} < T_{b,\text{dS}}$ because $\text{sech}(x)$ is a decreasing function for $x > 0$.
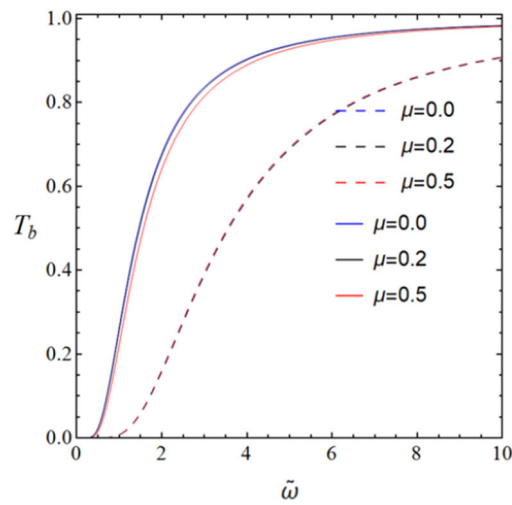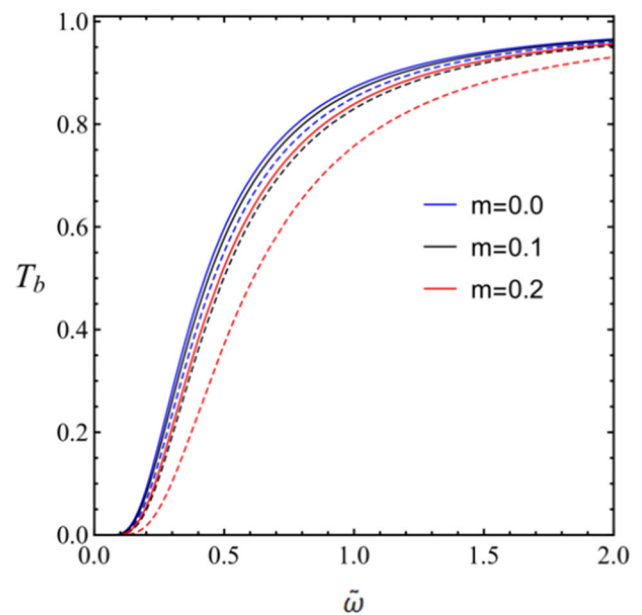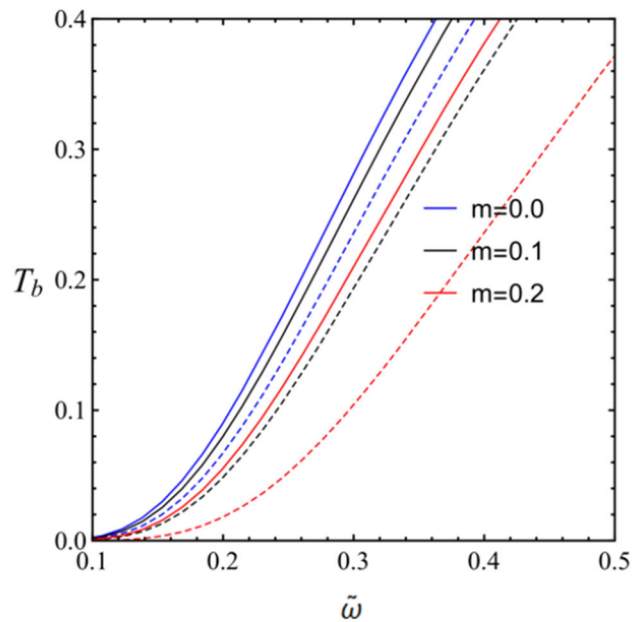
(a)
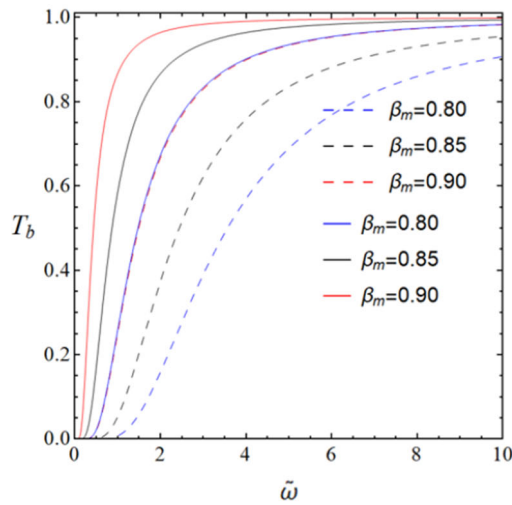
(b)

(c)

Fig. 11 Comparison of T_{app} and T_b defined in Eqs. (55) and (56), respectively, in the dS case
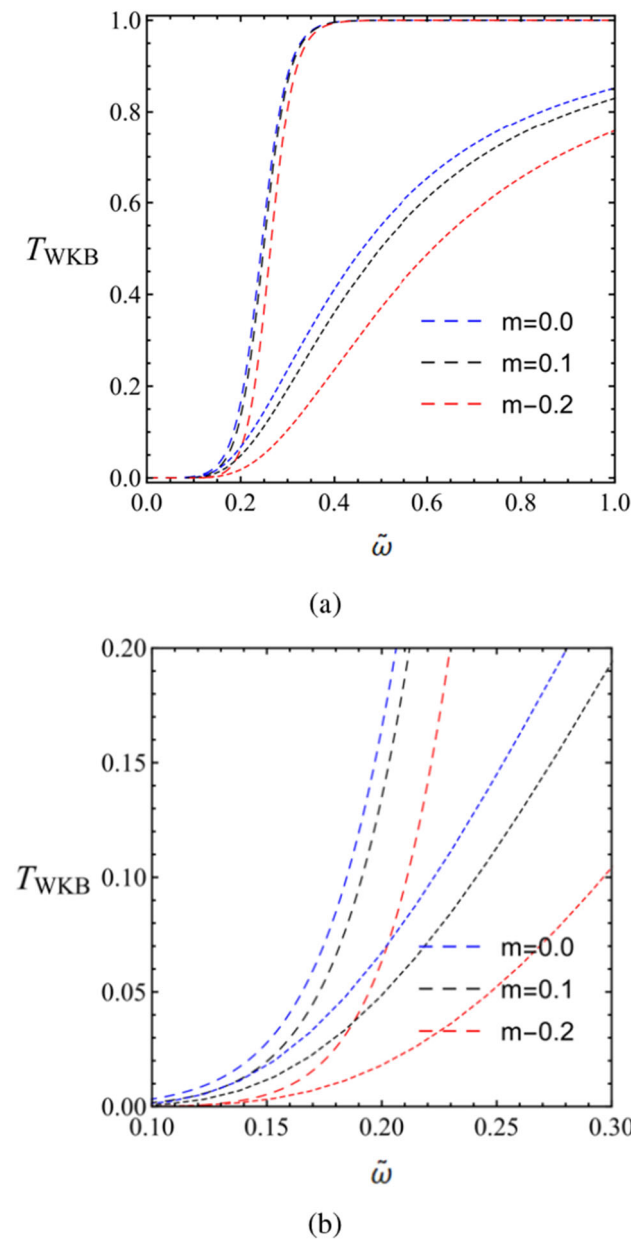

(a)

(b)

Fig. 12 **a** The bounds on the greybody factors of the SdS black holes (dashed line) and the asymptotically dS black holes in the dRGT massive gravity (solid line) for $c_2 = -0.01$, $\beta_m = 0.89$, $\ell = 1$ and $\tilde{m} = 0, 0.1$ and 0.2. **b** The magnification of **a**

Moreover, when m increases, both $T_{b,SdS}$ and $T_{b,dS}$ decreases. This is apparent because again sech(x) is a decreasing function for $x > 0$.

The results from the WKB approximation can be used for $\ell \neq 0$ as we mentioned above. The graphs of T_{WKB} compared to $T_{b,SdS,\ell=1}$ with different m for the SdS black holes are

(a)

(b)

Fig. 13 **a** The greybody factors of the SdS black holes $T_{b,\text{SdS},\ell=1}$ from the bound (dotted line) and T_{WKB} from the WKB method (dashed line) for $c_2 = -0.01$, $\ell = 1$ and $\tilde{m} = 0$, 0.1 and 0.2. **b** The magnification of **a**

(a)

(b)

Fig. 14 **a** The greybody factors of the asymptotically dS black holes in the dRGT massive gravity $T_{b,\text{dS},\ell=1}$ from the bound (solid line) and T_{WKB} from the WKB method (dashed line) for $c_2 = -0.01$, $\beta_m = 0.89$, $\ell = 1$ and $\tilde{m} = 0$, 0.1 and 0.2. **b** The magnification of **a**

plotted in Fig. 13. We see that $T_{b,\text{SdS},\ell=1} \leq T_{\text{WKB}}$, which indicates that $T_{b,\text{SdS},\ell=1}$ is a true lower bound. Moreover, T_{WKB} and $T_{b,\text{SdS},\ell=1}$ are so close to one another when $\tilde{\omega}$ is small.

The graphs of T_{WKB} compared to $T_{b,\text{dS},\ell=1}$ with different $\tilde{m}$ for the asymptotically dS black holes in the dRGT massive gravity are plotted in Fig. 14. We see that $T_{b,\text{dS},\ell=1} \leq T_{\text{WKB}}$, which indicates that $T_{b,\text{dS},\ell=1}$ is also a true lower bound. Moreover, T_{WKB} and $T_{b,\text{dS},\ell=1}$ are so close to one another when $\tilde{\omega}$ is small.

4.2 Greybody factors of the AdS black hole

An AdS black hole in the dRGT massive gravity can have more than one horizon, while a Schwarzschild AdS black hole has only one horizon. In this work, we are interested in the case where the AdS black hole has three horizons. Its potential is shown in Fig. 8, where the AdS potentials for $\ell = 0$ can be both positive and negative on $\tilde{r}_1 < \tilde{r} < \tilde{r}_2$ and $\tilde{r}_2 < \tilde{r} < \tilde{r}_3$, while one for $\ell \neq 0$ is positive on $\tilde{r}_1 <$

$\tilde{r} < \tilde{r}_2$ and negative on $\tilde{r}_2 < \tilde{r} < \tilde{r}_3$. Therefore, finding the bounds on the greybody factors for such two cases can be done independently.

4.2.1 $\ell = 0$

We divide the region of $\tilde{r}$ into two areas, $\tilde{r}_1 < \tilde{r} < \tilde{r}_2$ and $\tilde{r}_2 < \tilde{r} < \tilde{r}_3$. In the first region, $f_{\text{AdS}}(\tilde{r})$ is always positive. However, the AdS potential is positive for $\tilde{r}_1 < \tilde{r} < \tilde{r}_{1\text{cri}}$ and negative for $\tilde{r}_{1\text{cri}} < \tilde{r} < \tilde{r}_2$, where $\tilde{r}_{1\text{cri}}$ is the point satisfying $f'_{\text{AdS}}(\tilde{r}_{1\text{cri}}) = -\tilde{m}^2\tilde{r}_{1\text{cri}}$. From Eq. (50), we can write

$$T_{\text{AdS},\ell=0} \geq T_{\text{b, AdS},\ell=0}, \tag{72}$$

where

$$T_{\text{b, AdS},\ell=0} = \text{sech}^2\left[\frac{1}{2\tilde{\omega}}\int_{\tilde{r}_1}^{\tilde{r}_{1\text{cri}}} \frac{\tilde{V}_{\text{AdS},\ell=0}(\tilde{r})}{f_{\text{AdS}}(\tilde{r})}d\tilde{r}\right.$$
$$\left.-\frac{1}{2\tilde{\omega}}\int_{\tilde{r}_{1\text{cri}}}^{\tilde{r}_2} \frac{\tilde{V}_{\text{AdS},\ell=0}(\tilde{r})}{f_{\text{AdS}}(\tilde{r})}d\tilde{r}\right] \tag{73}$$

and $\tilde{V}_{\text{AdS},\ell=0}(\tilde{r})/f_{\text{AdS}}(\tilde{r})$ is

$$\frac{\tilde{V}_{\text{AdS},\ell=0}(\tilde{r})}{f_{\text{AdS}}(\tilde{r})} = \frac{2\tilde{M}}{\tilde{r}^3} + 2\alpha_g c_2 - \frac{3\alpha_g\sqrt[3]{4c_2^2}}{\tilde{r}} + \tilde{m}^2. \tag{74}$$

Calculating the integrals, we obtain

$$T_{\text{b, AdS},\ell=0} = \text{sech}^2\left[\frac{1}{2\tilde{\omega}}\left\{\tilde{M}\left(\frac{1}{\tilde{r}_1^2} + \frac{1}{\tilde{r}_2^2} - \frac{2}{\tilde{r}_{1\text{cri}}^2}\right)\right.\right.$$
$$-2\alpha_g c_2(\tilde{r}_1 + \tilde{r}_2 - 2\tilde{r}_{1\text{cri}})$$
$$-3\alpha_g\sqrt[3]{4c_2^2}\ln\frac{\tilde{r}_{1\text{cri}}^2}{\tilde{r}_1\tilde{r}_2}$$
$$\left.\left.-\tilde{m}^2(\tilde{r}_1 + \tilde{r}_2 - 2\tilde{r}_{1\text{cri}})\right\}\right]. \tag{75}$$

The bounds on the greybody factors with different $\tilde{m}$, β_m and c_2 are plotted in Fig. 15a, c, d, respectively. In Fig. 15a, we see when the scalar mass increases, the greybody factor bound keeps increasing until $\tilde{m} = 0.8$ and then decreasing for $\tilde{m} > 0.8$. In fact, by performing in the same way as done in the dS case, we found that there exists a critical mass in which the greybody bound is maximum. For example, by setting $\tilde{M} = 1$, $\alpha_g = 1$, $c_2 = 1$, and $\beta_m = 1.08$, we found that the critical mass is at $m_c = 0.7937$. This can be seen by considering the area under the function $|V/f|$ as found in Fig. 15b.

For Fig. 15c, we see that when β_m increases, the bound on the greybody factors decreases. This is interesting because from Fig. 7a, the local maximum of the potential also decreases with increasing β_m. The changes in the AdS potential and the AdS bound with β_m are the same. This is due to the fact that the behaviour of the bound of the greybody factor

is controlled by the area under the curve of function $|V/f|$, not $|V|$ as we have discussed above.

For Fig. 15d, we see that when c_2 increases, the bound on the greybody factors decreases. For the background of the stronger cosmological constant, the massive scalar field can be harder to transmit from the AdS potential.

The graphs of T_{app} with different $\tilde{m}$, β_m and c_2 are plotted in Fig. 16a–c, respectively. In Fig. 16a, the result is interesting. When $\tilde{m}$ increases to 0.2, the bound also increases. However, if $\tilde{m}$ continues to increase, the bound starts to decrease. We see that the blue curve ($\tilde{m} = 0$) is below the grey curve ($\tilde{m} = 0.2$), but above the red curve ($\tilde{m} = 0.5$). For the low mass, the more massive scalar field can better be transmitted from the AdS potential. However, for the high mass, the more massive scalar field can be more difficult to transmit from the AdS potential.

For Fig. 16b, we see that when β_m increases, the bound on the greybody factors decreases. This is interesting because from Fig. 7a, the local maximum of the potential also decreases with increasing β_m. The changes in the AdS potential and the AdS bound with β_m are the same.

For Fig. 16c, the result is also interesting. We see that when c_2 increases to 1/2, the bound on the greybody factors also increases. However, if c_2 continues to increase, the bound starts to decrease. We see that the red curve ($c_2 = 1/3$) is below the grey curve ($c_2 = 1/2$), but above the blue curve ($c_2 = 1$). For the background of the weak cosmological constant, the massive scalar field can better be transmitted from the AdS potential. However, for the background of the strong cosmological constant, the massive scalar field can be transmitted from the AdS potential, but with more difficulty.

Moreover, we explicitly see that T_{app} (the solid curve) is greater than or equal to T_{b} (the dash curve) according to inequality (57).

In the second region, where $\tilde{r}_2 < \tilde{r} < \tilde{r}_3$, $f_{\text{AdS}}(\tilde{r})$ is negative. Moreover, the AdS potential is positive for $\tilde{r}_2 < \tilde{r} < \tilde{r}_{2\text{cri}}$ and negative for $\tilde{r}_{2\text{cri}} < \tilde{r} < \tilde{r}_3$, where $\tilde{r}_{2\text{cri}}$ is the point satisfying $f'_{\text{AdS}}(\tilde{r}_{2\text{cri}}) = -\tilde{m}^2\tilde{r}_{2\text{cri}}$. From Eq. (50), we can write

$$T_{\text{AdS}} \geq \text{sech}^2\left[\frac{1}{2\tilde{\omega}}\int_{\tilde{r}_2}^{\tilde{r}_{2\text{cri}}} \frac{\tilde{V}_{\text{AdS}}(\tilde{r})}{f_{\text{AdS}}(\tilde{r})}d\tilde{r}\right.$$
$$\left.-\frac{1}{2\tilde{\omega}}\int_{\tilde{r}_{2\text{cri}}}^{\tilde{r}_3} \frac{\tilde{V}_{\text{AdS}}(\tilde{r})}{f_{\text{AdS}}(\tilde{r})}d\tilde{r}\right], \tag{76}$$

where $\tilde{V}_{\text{AdS}}(\tilde{r})/f_{\text{AdS}}(\tilde{r})$ is

$$\frac{\tilde{V}_{\text{AdS}}(\tilde{r})}{f_{\text{AdS}}(\tilde{r})} = \frac{\ell(\ell+1)}{\tilde{r}^2} + \frac{2\tilde{M}}{\tilde{r}^3} + 2\alpha_g c_2 - \frac{3\alpha_g\sqrt[3]{4c_2^2}}{\tilde{r}} + \tilde{m}^2. \tag{77}$$

(a)

(b)

(c)

(d)
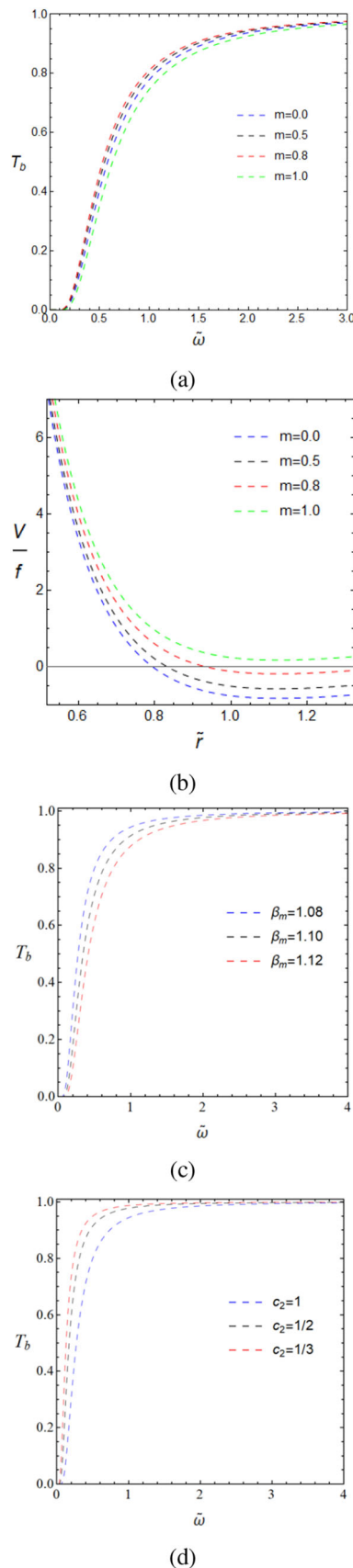
◀**Fig. 15** The rigorous bounds (between $\tilde{r}_1$ and $\tilde{r}_2$) on the greybody factors of the AdS black holes with $\ell = 0$, $\tilde{M} = 1$, $\alpha_g = 1$. **a** $c_2 = 1$, $\beta_m = 1.08$ and $\tilde{m} = 0$, 0.2 and 0.5. **b** The graph of the function $\tilde{V}/f$ in the AdS case with the same parameters. **c** $c_2 = 1$, $\tilde{m} = 0.2$ and $\beta_m = 1.08$, 1.10 and 1.12. **d** $\tilde{m} = 0.2$, $\beta_m = 1.08$ and $c_2 = 1$, 1/2 and 1/3

Calculating the integrals, we obtain

$$
\begin{aligned}
T_{\text{AdS}} \geq \text{sech}^2 \Bigg[\frac{1}{2\tilde{\omega}} \Bigg\{ & \ell(\ell+1) \left(\frac{1}{\tilde{r}_2} + \frac{1}{\tilde{r}_3} - \frac{2}{\tilde{r}_{2\text{cri}}} \right) \\
& + \tilde{M} \left(\frac{1}{\tilde{r}_2^2} + \frac{1}{\tilde{r}_3^2} - \frac{2}{\tilde{r}_{2\text{cri}}^2} \right) \\
& - 2\alpha_g c_2 (\tilde{r}_2 + \tilde{r}_3 - 2\tilde{r}_{2\text{cri}}) \\
& - 3\alpha_g \sqrt[3]{4c_2^2} \ln \frac{\tilde{r}_{2\text{max}}^2}{\tilde{r}_2 \tilde{r}_3} \\
& - \tilde{m}^2 (\tilde{r}_2 + \tilde{r}_3 - 2\tilde{r}_{2\text{cri}}) \Bigg\} \Bigg].
\end{aligned}
\tag{78}
$$

The bounds on the greybody factors with different $\tilde{m}$, β_m and c_2 are plotted in Fig. 17a, c, d, respectively. In Fig. 17a, b, the bound increases with increasing $\tilde{m}$ until $\tilde{m} = 0.2$. After that, the bound starts to decrease with increasing $\tilde{m}$. We see that the blue curve ($\tilde{m} = 0$) is below the grey curve ($\tilde{m} = 0.2$), but above the red curve ($\tilde{m} = 0.5$). Actually, by performing a numerical method as done in the previous case, we found the critical mass for which the greybody factor bound is maximum. For example, in our parameter setting, $c_2 = 1$, $\beta_m = 1.08$, the critical mass can be obtained as $m_c = 0.186$.

For Fig. 17c, we see that when β_m increases, the bound on the greybody factors decreases. This follows from Fig. 7a where the absolute of the second local maximum and the second local minimum of the potential increases with increasing β_m.
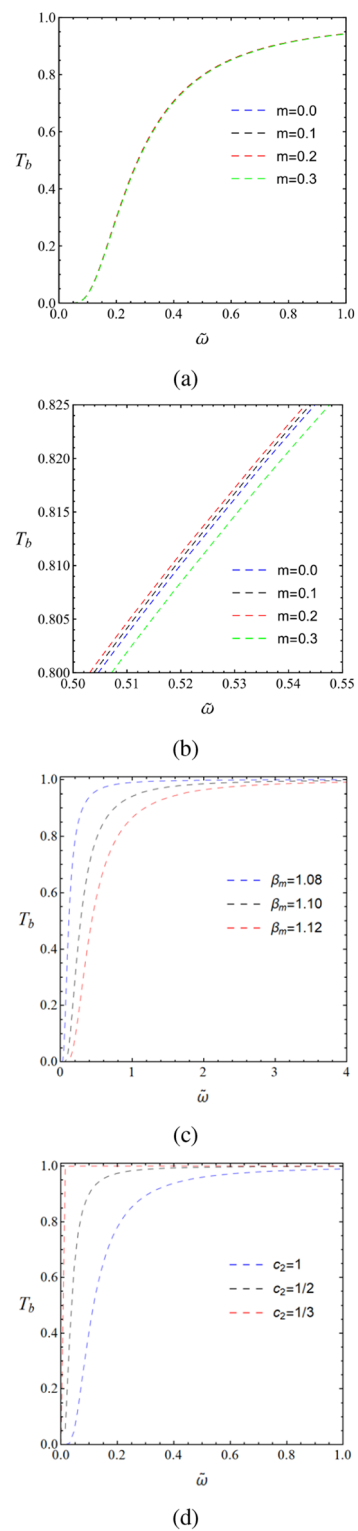
For Fig. 17d, we see that the bound on the greybody factors decreases with increasing c_2. This is the regular result because from Fig. 7b, the second local maximum increases with increasing c_2. In the background with the stronger cosmological constant, the massive scalar field can penetrate the AdS potential, but with more difficulty.

The graph of T_{app} with different $\tilde{m}$, β_m and c_2 are plotted in Fig. 18a–c, respectively. In Fig. 18a, we see that the bound decreases with increasing $\tilde{m}$. This result is interesting because from Fig. 6a, b, the second local maximum also decreases with increasing $\tilde{m}$. The changes in the second local maximum of the AdS potential and the AdS bound with $\tilde{m}$ are the same. The more massive scalar field can be harder to transmit from the AdS potential.

For Fig. 18b, we see that when β_m increases, the bound on the greybody factors also increases. This is interesting because from Fig. 7a, the second local maximum of the potential also increases with increasing β_m. Again, the changes in

(a)

(b)

(c)
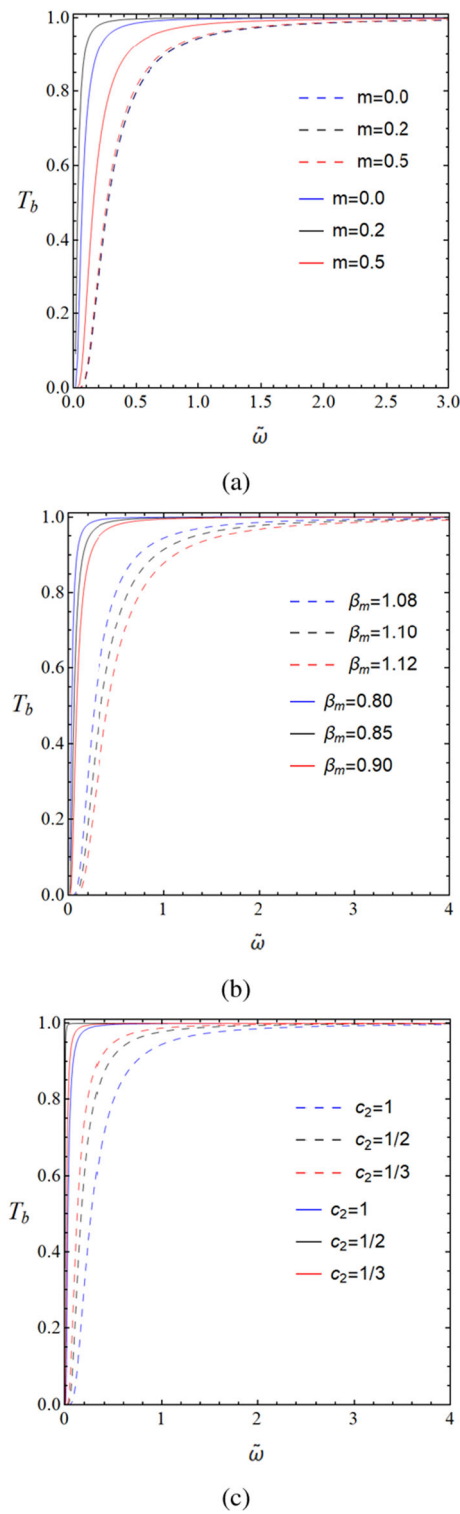
Fig. 16 The rigorous bounds (between $\tilde{r}_1$ and $\tilde{r}_2$) on the greybody factors for the AdS case with $\ell = 0$, $\tilde{M} = 1$, $\alpha_g = 1$. **a** $c_2 = 1$, $\beta_m = 1.08$ and $\tilde{m} = 0, 0.2$ and 0.5. **b** $c_2 = 1$, $\tilde{m} = 0.2$ and $\beta_m = 1.08$, 1.10 and 1.12. **c** $\tilde{m} = 0.2$, $\beta_m = 1.08$ and $c_2 = 1, 1/2$ and $1/3$. The solid line represents T_{app} and the dash line represents T_b

(a)

(b)

(c)

(d)

Fig. 17 The rigorous bounds (between $\tilde{r}_2$ and $\tilde{r}_3$) on the greybody factors of the AdS black holes with $\ell = 0$, $\tilde{M} = 1$, $\alpha_g = 1$. **a, b** $c_2 = 1$, $\beta_m = 1.08$ and $\tilde{m} = 0, 0.2$ and 0.5. **c** $c_2 = 1$, $\tilde{m} = 0.2$ and $\beta_m = 1.08$, 1.10 and 1.12. **d** $\tilde{m} = 0.2$, $\beta_m = 1.08$ and $c_2 = 1, 1/2$ and $1/3$

the second local maximum of the AdS potential and the AdS bound with β_m are the same.

For Fig. 18c, we see that the bound on the greybody factors decreases with increasing c_2. This is the regular result because from Fig. 7b, the second local maximum increases with increasing c_2. In the background with the stronger cosmological constant, the massive scalar field can penetrate the AdS potential, but with more difficulty.

Moreover, we explicitly see that T_{app} (the solid curve) is greater than or equal to T_b (the dash curve) according to the inequality (57).

4.2.2 $\ell \neq 0$

From Fig. 8, the AdS potential for $\ell \neq 0$ is positive on the interval $\tilde{r}_1 < \tilde{r} < \tilde{r}_2$ and negative on the interval $\tilde{r}_2 < \tilde{r} < \tilde{r}_3$. That is the AdS potential for $\ell \neq 0$ has the same sign as $f_{\text{AdS}}(\tilde{r})$. Therefore, from Eqs. (55) and (56), $T_b = T_{\text{app}}$. Then, Eq. (58) becomes

$$T_{\text{AdS},\ell \neq 0} \geq T_{b,\text{AdS},\ell \neq 0}, \tag{79}$$

where

$$T_{b,\text{AdS},\ell \neq 0} = \text{sech}^2 \left[\frac{1}{2\tilde{\omega}} \int_{\tilde{r}_1}^{\tilde{r}_2} \frac{\tilde{V}_{\text{AdS},\ell \neq 0}(\tilde{r})}{f_{\text{AdS}}(\tilde{r})} d\tilde{r} \right] \tag{80}$$

and

$$\frac{\tilde{V}_{\text{AdS},\ell \neq 0}(\tilde{r})}{f_{\text{AdS}}(\tilde{r})} = \frac{\ell(\ell + 1)}{\tilde{r}^2} + \frac{2\tilde{M}}{\tilde{r}^3} + 2\alpha_g c_2 - \frac{3\alpha_g \sqrt[3]{4c_2^2}}{\tilde{r}} + \tilde{m}^2. \tag{81}$$

Calculating the integrals, we obtain

$$T_{b,\text{AdS},\ell \neq 0} = \text{sech}^2 \left[\frac{1}{2\tilde{\omega}} \left\{ \ell(\ell + 1) \left(\frac{1}{\tilde{r}_1} - \frac{1}{\tilde{r}_2} \right) \right. \right.$$
$$\left. + \tilde{M} \left(\frac{1}{\tilde{r}_1^2} - \frac{1}{\tilde{r}_2^2} \right) + 2\alpha_g c_2 (\tilde{r}_2 - \tilde{r}_1) \right.$$
$$\left. \left. - 3\alpha_g \sqrt[3]{4c_2^2} \ln \frac{\tilde{r}_2}{\tilde{r}_1} + \tilde{m}^2 (\tilde{r}_2 - \tilde{r}_1) \right\} \right]. \tag{82}$$

The graphs of T_{WKB} compared to T_b between $\tilde{r}_2$ and $\tilde{r}_3$ with different $\tilde{m}$ are plotted in Fig. 19. Note that the results for one between $\tilde{r}_1$ and $\tilde{r}_2$ are similar to this case and we omit to present here. From this figure, we see that T_b is less than T_{WKB}, showing that T_b is a true lower bound. Note that they are so close to one another when $\tilde{\omega}$ is around 0.4. Moreover, their behaviors are similar. When $\tilde{m}$ increases, both T_{WKB} and T_b decrease.
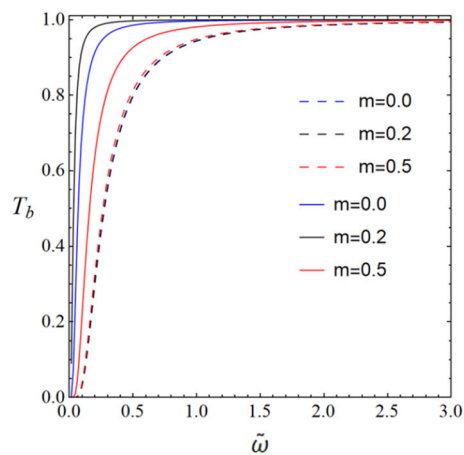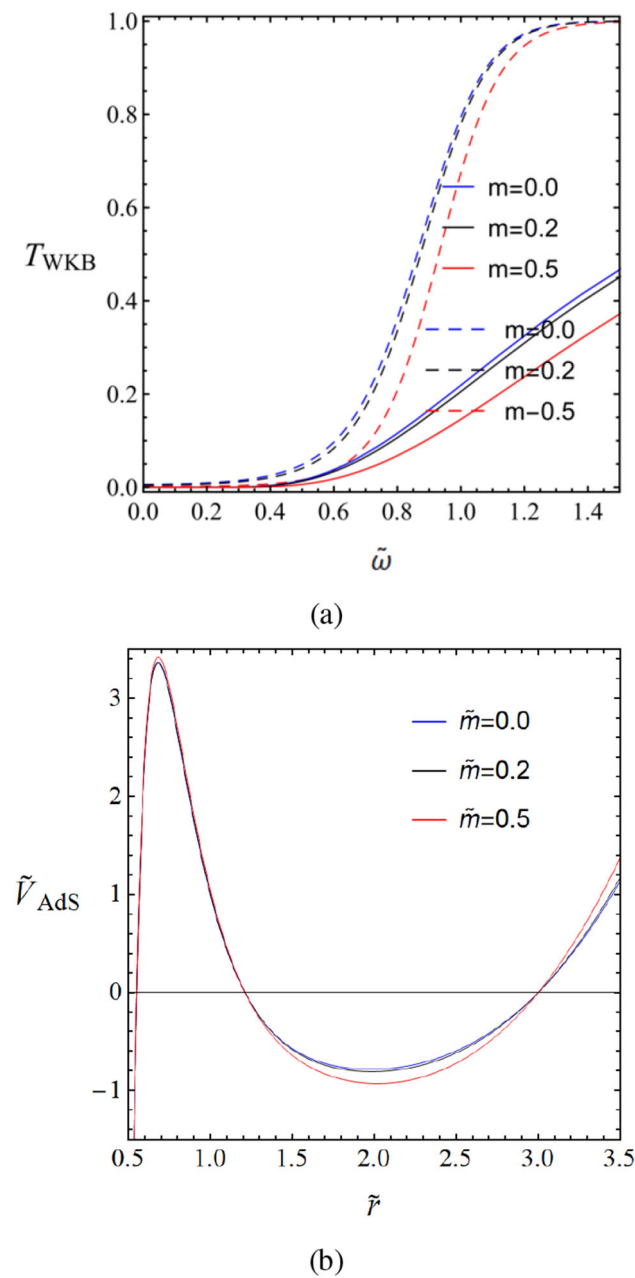
(a)
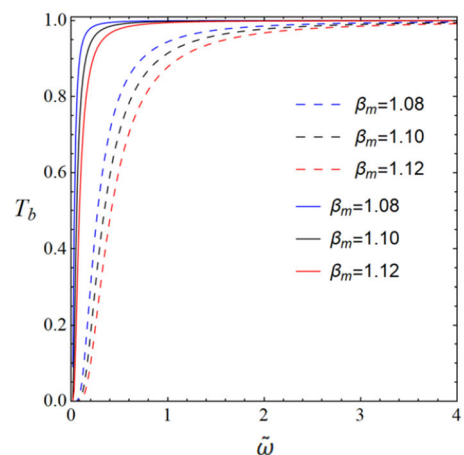
(b)
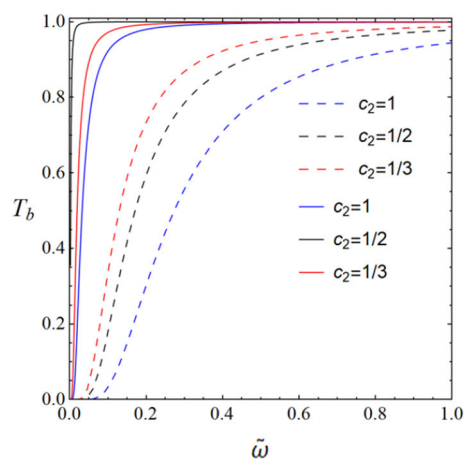
(c)

Fig. 18 The rigorous bounds (between $\tilde{r}_2$ and $\tilde{r}_3$) on the greybody factors of the AdS black holes with $\ell = 0$, $\tilde{M} = 1$, $\alpha_g = 1$. **a** $c_2 = 1$, $\beta_m = 1.08$ and $\tilde{m} = 0$, 0.2 and 0.5. **b** $c_2 = 1$, $\tilde{m} = 0.2$ and $\beta_m = 1.08$, 1.10 and 1.12. **c** $\tilde{m} = 0.2$, $\beta_m = 1.08$ and $c_2 = 1$, 1/2 and 1/3

(a)

(b)

Fig. 19 **a** The greybody factor between $\tilde{r}_2$ and $\tilde{r}_3$ of the AdS black holes, T_b from the bound (solid line) and T_{WKB} from the WKB method (dashed line) for $c_2 = 1$, $\beta_m = 1.1$, $\ell = 2$ and $\tilde{m} = 0$, 0.2 and 0.5. **b** The AdS potential with $c_2 = 1$, $\beta_m = 1.1$ and $\ell = 2$

5 Conclusion

One of the interesting issues of a black hole is that it behaves as a thermal system. Specifically, a black hole can carry entropy and can emit radiation called the Hawking radiation. Moreover, the spectrum of the radiations from black holes is the same as that of the black-body spectrum. It has also been found that the spacetime curvature can act as a potential barrier, which allows some of the radiation to transmit and

reflect as found in similar situations in quantum mechanics. As a result, the greybody factor is defined in order to take into account the transmission amplitude of the radiation from the black holes.

In this paper, we investigate the greybody factor for the massive scalar field from the dRGT black hole. In theories beyond GR, there are usually additional degrees of freedom that can be coupled to gravity. A simplest example is known as the scalar-tensor theory, in which a scalar field has couplings to gravity. In this sense, the scalar field may be one of the simple candidates for the Hawking radiation, making it an interesting issue to investigate the greybody factor for a massive scalar field. One of the interesting modified gravity theories is the dRGT massive gravity, since it is a candidate for describing the late-time expansion of the universe. Moreover, it turns out that there exists a black hole solution in the dRGT massive gravity. One of the interesting properties of the dRGT black hole is that it is possible to obtain the asymptotically dS/AdS spacetime, which can be distinguished from the SdS/SAdS black hole. Therefore, it is worthwhile to investigate the greybody factor from the dRGT black hole by analyzing how the mass of the scalar field influences the greybody factor.

In the present work, we begin with the review of the dRGT black hole, including the horizon structure of the black hole in both the asymptotically dS and the AdS spacetime. For the dRGT black hole with the asymptotically dS spacetime, there are generically two horizons. In order to characterize the existence of the horizon, we introduce the model parameter β_m in which $0 < \beta_m < 1$ for the existence of two horizons. This parameter also influences the structure of the horizon as the larger the value of the parameter, the narrower the width of the two horizons. Moreover, the strength of the cosmological constant can be characterized by parameter c_2. For the dS case, when $c_2 < 0$ the role of c_2 is the same as the cosmological constant. For example, the smaller the value of $|c_2|$, the wider width of the horizons. For the AdS case, we focus on the black hole with three horizons, which is distinguished from the SAdS black hole (only one horizon exists). In the same manner as the dS case, we are left with only two parameters to characterize the horizon structure where $1 < \beta_m < 2/\sqrt{3}$ is the condition for the existence of three horizons.

We find the potential, which acts as the barrier allowing the scalar field to transmit in a similar manner to quantum mechanics. Since the potential depends on the horizon function and its derivative, it is controlled by two parameters β_m and c_2. Moreover, there are two more parameters, the scalar field mass m and the multipole ℓ, to characterize the behaviour of the potential. It is found that the higher the value of the scalar field mass, the higher the value of the maximum potential. In fact, for both the dS and the AdS cases, the mass term contributes to the positive part of the potential, to shift

the potential upward. For the dS case, it is found that the potential from the dRGT black hole is narrower than one from the SdS black hole. This behaviour is inherited from the narrow width of the two horizons. For the AdS case, the potential from the dRGT black hole cannot be compared to one from SAdS, since the structure of the horizons are completely different. As for the multipole term, it also provides a positive contribution to the potential for which the potential will be shifted upward where the parameter ℓ is increased. It is found that for $\ell = 0$ with a small scalar field mass, there exists a negative part of the potential. In this case, we have to carefully consider the calculation for the greybody factor bound since the expression contains the absolute value of the potential.

The greybody factors from various kinds of spacetime geometry have been intensively investigated by various methods. One of the ways is finding solutions in the asymptotic regions and then matching the solutions at the boundaries. However, the solutions are mostly written in terms of special functions, which makes it difficult to analyze the behaviour of the spectrum analytically. Other interesting way, which is intensively investigated in literature, is that of using the WKB approximation. It provides a good approximation for a simple form of spacetime geometries, which then requires the higher potential, or in other words, requires high multipole. The other way to investigate the greybody factor is to consider the bound of the greybody factor instead of the exact one. This method allows us to study the behaviour of the greybody factor analytically.

For the dS case, the greybody factor depends on the shape of the potential as found in quantum mechanics. The scalar field mass provides a higher potential so that it is more difficult to transmit. Therefore, this provides a lower greybody factor. However, for the case $\ell = 0$ with a small scalar field mass, there exists a negative part of the potential. We found that there exists a critical mass which provides the maximum bound of the greybody factor. This is one of the crucial behaviour of the massive scalar field for the greybody factor. Note that this can be found in both the dRGT black hole and the SdS black hole. Moreover, we found that the greybody factor from the dRGT black hole is higher than one from the SdS black hole. This is due to the fact that the potential for the dRGT black hole is thinner than one for the SdS black hole. It is also found that the results of the greybody factor bound agree with ones from the WKB method.

For AdS case, the role of the scalar field mass is similar to the dS case in both systems between r_1 and r_2, and r_2 and r_3. The higher the mass, the higher the potential and the lower the greybody factor. However, for the case in which there exist both the negative and the positive part of the potential, e.g. $\ell = 0$ with the small scalar field mass, we found that there exists a critical mass which provides the maximum bound of the greybody factor. This is one of the crucial behaviour

of the massive scalar field for the greybody factor. We also found that the results of the greybody factor bound agree with ones from the WKB method.

References

1. S.W. Hawking, Particle creation by black holes. Commun. Math. Phys. **43**, 199–220 (1975)
2. M. Visser, Some general bounds for one-dimensional scattering. Phys. Rev. A **59**, 427 (1999)
3. P. Boonserm, Rigorous Bounds on Transmission, Reflection, and Bogoliubov Coefficients, Ph. D. Thesis. Victoria University of Wellington (2009)
4. P. Boonserm, M. Visser, Reformulating the Schrödinger equation as a Shabat–Zakharov system. J. Math. Phys. **51**, 022105 (2010)
5. P. Boonserm, M. Visser, Bounding the greybody factors for Schwarzschild black holes. Phys. Rev. D **78**, 101502(R) (2008)
6. T. Ngampitipan, P. Boonserm, Bounding the greybody factors for the Reissner–Nordström black holes. J. Phys. Conf. Ser. **435**, 012027 (2013)
7. T. Ngampitipan, P. Boonserm, Bounding the greybody factors for non-rotating black holes. Int. J. Mod. Phys. D **22**, 1350058 (2013)
8. P. Boonserm, T. Ngampitipan, M. Visser, Regge–Wheeler equation, linear stability, and greybody factors for dirty black holes. Phys. Rev. D **88**, 041502(R) (2013)

9. P. Boonserm, T. Ngampitipan, M. Visser, Spin one Hawking radiation from dirty black holes. Int. J. Eng. Math. Phys. Sci. **7**, 1689–1693 (2013)

10. P. Boonserm, T. Ngampitipan, M. Visser, Bounding the greybody factors for scalar field excitations on the Kerr–Newman spacetime. J. High Energy Phys. **2014**, 113 (2014)

11. P. Boonserm, A. Chatrabhuti, T. Ngampitipan, M. Visser, Greybody factors for Myers–Perry black holes. J. Math. Phys. **55**, 112502 (2014)

12. T. Ngampitipan, P. Boonserm, Transmission probability for charged dilatonic black holes in various dimensions. JPS Conf. Proc. **1**, 013100 (2014)

13. T. Ngampitipan, Rigorous bounds on greybody factors for various types of black holes, PhD Thesis. Chulalongkorn University (2014)

14. T. Ngampitipan, P. Boonserm, M. Visser, Spin zero Hawking radiation for non-zero-angular momentum mode. AIP Conf. Proc. **1660**, 050066 (2015)

15. T. Ngampitipan, P. Boonserm, A. Chatrabhuti, P. Wongjun, Spin-zero Hawking radiation: Bounds on the zero-angular-momentum mode emission from Myers–Perry black holes. Malays. J. Math. Sci. **10**, 337–345 (2016)

16. P. Boonserm, T. Ngampitipan, P. Wongjun, Bounding the greybody factor, temperature and entropy of black holes in dRGT massive gravity. Am. J. Phys. Appl. **4**, 64–70 (2016)

17. T. Ngampitipan, P. Boonserm, A. Chatrabhuti, M. Visser, The rigorous bound on the transmission probability for massless scalar field of non-negative-angular-momentum mode emitted from a Myers–Perry black hole. AIP Conf. Proc. **1739**, 020020 (2016)

18. T. Ngampitipan, P. Boonserm, A. Chatrabhuti, M. Visser, Rigorous bounds on greybody factors: scalar emission of negative angular momentum modes from Myers–Perry black holes. Int. J. Eng. Technol. **8**, 311–314 (2016)

19. P. Boonserm, T. Ngampitipan, P. Wongjun, Greybody factor for black string in dRGT massive gravity. Eur. Phys. J. C **79**, 330 (2019)

20. K. Sansuk, P. Boonserm, T. Ngampitipan, Greybody factors for various black holes in perfect fluid spheres. Int. J. Math. Comput. Sci. **16**, 977–988 (2021)

21. P. Boonserm, C.H. Chen, T. Ngampitipan, P. Wongjun, Greybody factor for massive fermion emitted by a black hole in de Rham–Gabadadze–Tolley massive gravity theory. Phys. Rev. D **104**, 084054 (2021)

22. R.A. Konoplya, A.V. Zhidenko, Decay of massive scalar field in a Schwarzschild background. Phys. Lett. B **609**, 377–384 (2005)

23. H. Furuhashi, Y. Nambu, Instability of massive scalar fields in Kerr–Newman spacetime. Prog. Theor. Phys. **112**, 983–995 (2004)

24. H.S. Vieira, V.B. Bezerra, C.R. Muniz, Instability of the charged massive scalar field on the Kerr–Newman black hole spacetime. Eur. Phys. J. C **82**, 932 (2022)

25. J.D. Bekenstein, M. Schiffer, The many faces of superradiance. Phys. Rev. D **58**, 064014 (1998)

26. A. Ohashi, M. Sakagami, Massive quasi-normal mode. Class. Quantum Gravity **21**, 3973 (2004)

27. H. Koyama, A. Tomimatsu, Asymptotic tails of massive scalar fields in a Schwarzschild background. Phys. Rev. D **64**, 044014 (2001)

28. S. Deser, R. Jackiw, S. Templeton, Topologically massive gauge theories. Ann. Phys. **140**, 372–411 (1982)

29. E.A. Bergshoeff, O. Hohm, P.K. Townsend, Massive gravity in three dimensions. Phys. Rev. Lett. **102**, 201301 (2009)

30. V.I. Ogievetsky, I.V. Polubarinov, Interacting field of spin 2 and the Einstein equations. Ann. Phys. **35**, 167–208 (1965)

31. S. Mukohyama, M.S. Volkov, The Ogievetsky–Polubarinov massive gravity and the benign Boulware–Deser mode. JCAP **10**, 037 (2018)

32. T.L. Curtright, H. Alshal, Massive dual spin 2 revisited. Nucl. Phys. B **948**, 114777 (2019)

33. H. Alshal, T.L. Curtright, Massive dual gravity in N spacetime dimensions. J. High Energy Phys. **9**, 63 (2019)

34. C. de Rham, G. Gabadadze, A.J. Tolley, Resummation of massive gravity. Phys. Rev. Lett. **106**, 231101 (2011)

35. C. de Rham, Massive gravity. Living Rev. Relativ. **17**, 7 (2014)

36. S.G. Ghosh, L. Tannukij, P. Wongjun, A class of black holes in dRGT massive gravity and their thermodynamical properties. Eur. Phys. J. C **76**, 119 (2016)

37. P. Boonserm, T. Ngampitipan, P. Wongjun, Greybody factor for black holes in dRGT massive gravity. Eur. Phys. J. C **78**, 492 (2018)

38. M.S. Volkov, Self-accelerating cosmologies and hairy black holes in ghost-free bigravity and massive gravity. Class. Quantum Gravity **30**, 184009 (2013)

39. H. Zhang, X.Z. Li, Ghost free massive gravity with singular reference metrics. Phys. Rev. D **93**, 124039 (2016)

40. S.H. Hendi, R.B. Mann, S. Panahiyan, B.E. Panah, Van der Waals like behavior of topological AdS black holes in massive gravity. Phys. Rev. D **95**, 021501(R) (2017)

41. S.A. Fulling, *Aspects of Quantum Field Theory in Curved Space-Time* (Cambridge University Press, Cambridge, 1996), p.117

42. P. Lange, Calculation of Hawking radiation as quantum mechanical tunneling, Thesis. Uppsala Universitet (2007)

43. S. Iyer, C.M. Will, Black hole normal modes: a WKB approach. 1. Foundations and application of a higher order WKB analysis of potential barrier scattering. Phys. Rev. D **35**, 3621 (1987). https://doi.org/10.1103/PhysRevD.35.3621

44. H.T. Cho, Y.C. Lin, WKB analysis of the scattering of massive Dirac fields in Schwarzschild black hole spacetimes. Class. Quantum Gravity **22**, 775–790 (2005). https://doi.org/10.1088/0264-9381/22/5/001. arXiv:gr-qc/0411090 [gr-qc]